



## Invited Review Article

# A critical review on petrogenetic, metallogenic and geodynamic implications of granitic rocks exposed in north and east China: New insights from apatite geochemistry



Tehseen Zafar<sup>a,b,c,\*</sup>, Hafiz Ur Rehman<sup>d</sup>, Munazzam Ali Mahar<sup>e</sup>, Masroor Alam<sup>f</sup>,  
Abiola Oyebamiji<sup>a</sup>, Saif Ur Rehman<sup>c</sup>, Cheng-Biao Leng<sup>a,g</sup>

<sup>a</sup> State Key Laboratory of Ore Deposit Geochemistry, Institute of Geochemistry, Chinese Academy of Sciences, Guiyang, 550081, China

<sup>b</sup> University of Chinese Academy of Sciences, Beijing, 100049, China

<sup>c</sup> Institute of Geology, University of the Punjab, Lahore, 54590, Pakistan

<sup>d</sup> Department of Earth and Environmental Sciences, Kagoshima University, Kagoshima, 890-0065, Japan

<sup>e</sup> Department of Geological Sciences, University of Texas at El Paso, El Paso, TX, 79968, United States

<sup>f</sup> Department of Earth Sciences, Karakoram International University, Gilgit, 15100, Pakistan

<sup>g</sup> State Key Laboratory of Nuclear Resources and Environment, East China University of Technology, Nanchang, 330013, China

## ARTICLE INFO

## Keywords:

Magmatic  
Apatite  
Luming and LYRB granites  
Petrogenetic characteristics  
Mineralization  
Geodynamic  
evolution

## ABSTRACT

Apatite is significant phosphate-bearing accessory mineral that is omnipresent in most granitic rocks. In this study, we present geochemical characteristics of magmatic apatites from the Luming and Lower Yangtze granitic belts of NE and eastern China to explore their potential in petrogenesis, mineralization and tectonic evolution of granites. The petrogenetic, metallogenic and tectonic aspects of these granites remain subjects of great debate. This review aims to clarify these issues based on apatite geochemistry. The investigated apatites from both these localities are mainly fluorapatites reflecting the actual attributes of parental melts. Apatites from Luming and Lower Yangtze River Belt (LYRB) exhibit strong negative Eu anomalies suggesting plagioclase crystallization earlier than apatite. The negative correlation of  $\text{Eu}/\text{Eu}^*$  ( $\delta\text{Eu}$ ) vs Mn,  $\delta\text{Eu}$  vs  $\delta\text{Ce}$  and  $\delta\text{Eu}$  vs Ga in the apatites signifies that the parental magmas of both granites are produced under moderate reduced conditions. The Sr contents and REEs ratios in apatites serve as significant proxies to trace the differentiation history of Luming and Lower Yangtze granitic plutons. The apatites Sr/Y ratios vs  $\delta\text{Eu}$  also exhibit that both granites are non-adakitic in nature which is consistent with the host rocks non-adakitic affinities. Halogen data indicates that apatites of Lower Yangtze comprising more chlorine (0.02–1.45 wt.%) and less fluorine (1.51–3.85 wt.%) are linked with slab dehydration whereas apatites from Luming having lower Cl (0–0.04 wt.%) and higher F contents (3.36–5.29 wt.%) suggest association of granites with partial melting of juvenile crust material. Based on the positive correlation of  $\text{SO}_3$  with Li,  $(\text{La}/\text{Sm})_N$  vs  $(\text{Yb}/\text{Sm})_N$  and obvious variations of  $(\text{La}/\text{Yb})_N$  vs  $\text{Eu}/\text{Eu}^*$ , it is inferred that these host rocks are ore-associated. Furthermore, geochemical signatures of apatites from LYRB show low F/Cl ratios, stable La/Sm ratios, high  $\delta\text{Eu}$  (0.04–0.43, average 0.21) and low  $\delta\text{Ce}$  values (0.96–1.12, average 1.02) indicating that the magmas of these granites have association with slab dehydration and linked with Cu–Mo–W mineralization, induced from the mutual impacts of Paleo-Pacific plate subduction and intraplate extension. In comparison, fairly high F/Cl ratios, La/Sm ratios, low  $\delta\text{Eu}$  (0.12–0.23, average 0.16), high  $\delta\text{Ce}$  values (0.98–1.09, average 1.04) and low Sr/Th ratios of Luming apatites infer that the Mo–W bearing granites are originated in consequence of partial melting of juvenile crustal material. Based on apatite geochemistry, we document first time varieties of ore deposits specifically Mo–W and Cu deposit in LYRB and Mo–W deposit in Luming which are developed under lower oxygen fugacity. The compiled geochemical data and interpretations propose that apatite chemical constituents are worthwhile to pinpoint polymetallic mineralization and fingerprint for ore types. In view of these findings, we confirm that apatite is not only consistent to trace geological facts about parental magma characteristics but also a reliable pointer of geodynamic evolution and ore varieties.

\* Corresponding author at: State Key Laboratory of Ore Deposit Geochemistry, Institute of Geochemistry, Chinese Academy of Sciences, Guiyang, 550081, China.  
E-mail address: [zafar@vip.gyig.ac.cn](mailto:zafar@vip.gyig.ac.cn) (T. Zafar).

<https://doi.org/10.1016/j.jog.2020.101723>

Received 12 July 2019; Received in revised form 28 February 2020; Accepted 6 March 2020

Available online 15 April 2020

0264-3707/ © 2020 Elsevier Ltd. All rights reserved.

## 1. Introduction

Apatite is a significant accessory mineral and most ubiquitous phosphate phase in granitic rocks which is considered as a prominent source for rare earth elements (REEs), volatiles, strontium, phosphorus, uranium and substantial amounts of thorium (Chen and Simonetti, 2014; Webster and Piccoli, 2015). These specific elements are certainly accommodated in lattice of apatite (She et al., 2016). Apatite crystallizes from melts and constituents of apatite indicate extreme stability in the case of metamorphic as well as hydrothermal reactions (Creaser and Gray, 1992). Therefore, it remains stable in an extensive and diverse range of geologic conditions and processes (Watson, 1980). Apatite is not vulnerable to hydrothermal and metamorphic activities, hence, magmatic apatite can conceivably act as a proxy to trace attributes concerning the nature of its parental magma (Webster and Piccoli, 2015). This particular mineral can effectively record and sustain geological facts regarding magmatic and post-magmatic processes because of its primary genesis (Lisowiec et al., 2013). It can retain dynamic geological information relating to the crystallization process, which is critical to control the source of magma (Mitchell et al., 2017).

Technically, apatite is an important collector and concentrator of different elements that preferentially incorporates a suite of several elements such as alkali, transition, rare earth elements, and volatile components in its structural framework, making it worthwhile tool for broad range of geochemical approaches. On account of several replacements in its structure, apatite comprises multiple elements and thus can be valuable for evaluation of magmatic evolutionary processes (Chu et al., 2009; Szopa et al., 2013), compositional determination of volatiles (Zhu and Sverjensky, 1992), appraisal of oxygen fugacity (Marks et al., 2014) and radiometric and fission track dating (Chew and Donelick, 2012; Henrichs et al., 2018). Furthermore, apatite composition shows a vital role in mineral exploration and investigation of the origin of magmatic-hydrothermal deposits (Mao et al., 2016). Porphyry deposits are considered as one of the most worthwhile deposits at the global level. Apatite in these deposits crystallizes from hydrothermal fluids and melts, therefore, it can provide perceptions regarding hydrothermal conditions and magmatic history. Likewise, magmatic volatiles in apatite framework, for instance, Cl, S, F, and C deliver leading implications regarding passage and precipitation of numerous metals, pondered as a powerful and sensitive tool to track the amounts of volatile in the melt, which reflect its source characteristics (Mao et al., 2016). Thus, apatite composition serves as a significant tool to achieve a noteworthy conception about the metallogensis of porphyry Cu–Mo deposits. Moreover, geochemical features of apatites are important to document petrogenesis of granitic rocks. In particular, this leading mineral can contribute as a remarkable tool and applicable probe to infer implications for varieties of economic deposits associated with granitic rocks (Krneta et al., 2016; Zafar et al., 2019) and redox conditions of parental magma (Pan et al., 2016). Specific apatite trace elements containing LREE, Th, Y, Eu, Mn, Sr, and Ce can be suitable to deduce the magma chemistry as well as oxidation and reductive conditions of the parental melt (Cao et al., 2012). Therefore, the chemistry of apatite can contribute as an essential proxy to determine petrogenetic characteristics of parental magmas of plutons such as Luming and Lower Yangtze granites. Apart from this, the chemical compositions of apatites act as an important recorder in granitic rocks to provide new and vital metallogenic facts. Meanwhile, apatite constituents and its geochemical features are measured as exceptional fertility index that can be worthwhile as an exploration tool to discriminate barren and fertile reduced as well as oxidized granitic bodies (Zafar et al., 2019).

In consideration of the high-class properties of apatite, the chemistry of apatite is very dynamic to achieve better perceptions concerning petrogenetic attributes and mineralization potential of several commercial deposits. Therefore, to evaluate its applicability and present some new implications, we have nominated apatite bearing granites from Lower Yangtze River Belt (LYRB) and porphyry granites exposed

in the Luming area, NE China. Chen and Zhang, 2018 and Jiang et al., 2018a presented apatite geochemistry to explore petrogenesis of granites in areas of Luming and Lower Yangtze River Belt (LYRB) respectively. The petrogenetic and mineralization inferences about Luming granites are very limited; however, regarding A-type granites of LYRB, no investigation has been conducted so far in terms of metallogenic specificity and inclusive petrogenetic as well as tectonic implications are also not researched yet, based on apatite geochemistry. Therefore, using their geochemical data, we present here a comprehensive review status and shed new light and insights concerning petrogenetic and metallogenic characteristics of granitic bodies of Luming and LYRB. With these geochemical data we attempt to evaluate the apatite applications in petrogenesis and mineralization by answering the following three questions: (1) Are the variations between LYRB and Luming granitic rocks reflected by differences in apatite compositions? (2) To what degree does apatite express parental magma attributes of LYRB and Luming plutons? And (3) Can apatite constituents serve as a proxy to identify mineralization and regional metallogeny of both granitic rocks and deliver facts on the geodynamic evolution of LYRB and Luming plutons?

The consequences and objectives of our research stated in this review article substantiate that magmatic apatite is not only consistent to trace geological facts about parental magma characteristics but also a reliable pointer of tectonic environment and fingerprint for ore varieties. We expect that the present study can deliver an avenue for further research about mineralization potential, geodynamic evolution and parental magma attributes through apatite geochemistry.

## 2. Geological background of LYRB

The Lower Yangtze River Belt (LYRB) is situated on the NE boundary of the Yangtze Block (Fig. 1), adjoining to an orogenic belt named Dabie–Sulu. In the NW part, it is bounded by Tancheng–Lujiang and Xiangfan–Guangji Faults, and in the south, alienated from Cathaysia Block through Jiang–Shao Fault (Fig. 1). The Xiangfan–Guangji Fault isolates the LYRB from the Triassic Dabie Orogenic Belt. Its SE periphery is demarcated through Yangxing–Changzhou Fault that splits the LYRB from the Jiangnan territory, however, its NW margin is delineated via Tanlu Fault which alienates the LYRB from Dabie Orogenic Belt and North China Craton (Fig. 1). The LYRB is a vital belt of metallogenic characteristics which is represented through widespread late Mesozoic magmatic activities and broad varieties of ores are documented, therefore, considered as significant and potential area of massive magmatism and mineralization (Mao et al., 2011; Sun et al., 2012; Li et al., 2013). Field studies integrated with geochemical investigations indicated three events of magmatism in the Lower Yangtze. These main pulses of magmatic activities are documented as: (1) first phase is linked with Cu–Au–Mo mineralization which developed in 148–133 Ma and characterized by presence of host intrusions having intermediate to acidic nature of composition (Mao et al., 2006; Sun et al., 2003); (2) magnetite and apatite deposits developed in second phase (133–127 Ma), represented by occurrence of host rocks including basic-intermediate alkaline volcanic bodies (Mao et al., 2006; Zhou et al., 2011); (3) in the last period (125 Ma) uranium and gold-bearing A-type granites (Jiang et al., 2018b).

According to Jiang et al., 2018b, A-type granites of LYRB are apatite bearing and mainly developed in an extensional environment owing to lithospheric mantle thinning and asthenosphere upwelling. Diverse source components prompted through the convergence of Palaeo-Pacific plate beneath Southeast China, showed an important character in the development of A-type granites. The varieties of these granites promoted in the hot, reduced environment as well as cold and oxidized settings. These A-type granites are exposed randomly, express parallel magmatic belts and its sub-groups A<sub>1</sub> and A<sub>2</sub>-type granites are consecutively dispersed (Su et al., 2013 Fig. 1).

From east to west, the apatite bearing A<sub>1</sub> and A<sub>2</sub>-type plutons are

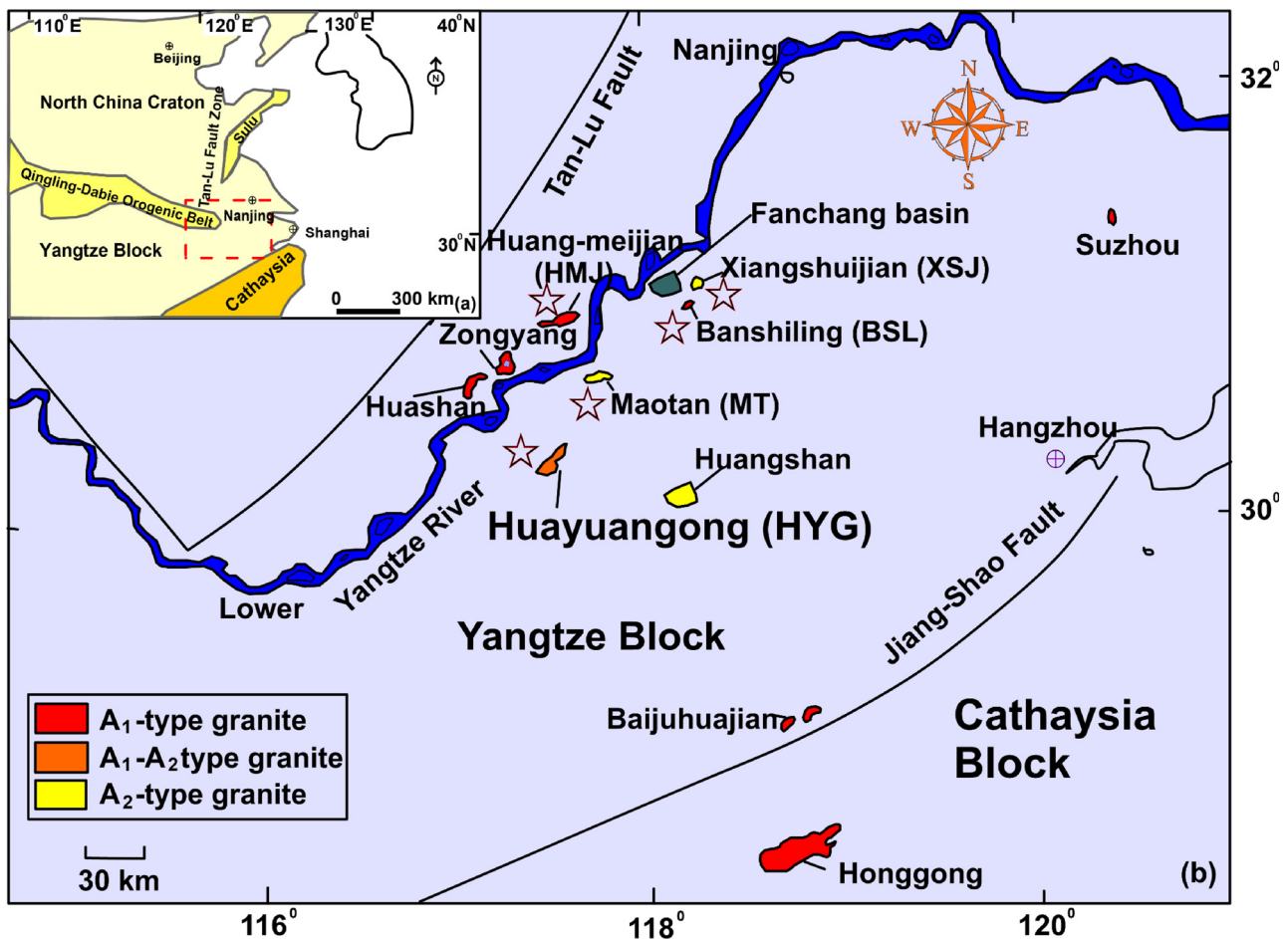


Fig. 1. Geological map of Lower Yangtze River Belt (LYRB). (a) Tectonic map of eastern China. (b) Location and distribution of A-type granitic bodies in LYRB (modified from Jiang et al., 2018a), BSL (Banshiling), XSJ (Xiangshuijian), HYG (Huayuangong) and MT (Maotan) on the southern and HMJ (Huangmeijian) granites on the northern bank of the LYRB.

documented as Banshiling (BSL  $A_1$ ), Xiangshuijian (XSJ  $A_2$ ), Maotan (MT  $A_2$ ), Huayuangong (HYG  $A_1$ ,  $A_2$ ) and Huangmeijian (HMJ  $A_1$ ), respectively (Ling et al., 2009; Li et al., 2011; Jiang et al., 2018a). These varieties of Early Cretaceous are collectively named as A-type granites of the LYRB. The description of each A-type plutonic body can be illustrated as follows.

The BSL  $A_1$  pluton covers an area of approximately 16 km<sup>2</sup> and it is situated adjacent to the XSJ granite. This type of granite is widely exposed in the SE part of Fanchang Basin (Fig. 1; Lou and Du, 2006). Petrographically, this variety is characterized as quartz monzonite comprising 41–51 % microcline, 32–39 % plagioclase, 11–17 % quartz and 4–9 % "biotite" (Fig. 2a).

The XSJ  $A_2$  pluton is situated at the SE portion of the Fanchang Basin (Fig. 1) and observed as alkali-feldspar rich granitic rock based on thin section study (Fig. 2b). Mineralogically, the rock contains 62–68 % microcline, 24–29 % quartz, 4–9 % "biotite" and 3–6 % plagioclase.

The MT and HYG granites are located in the Anqing-Guichi region and both of these varieties are documented at the transitional portion of  $A_1$  and  $A_2$ -type pluton zones (Fig. 1; Li et al., 2012b). Microscopically, the MT pluton reveals graphic and porphyritic textural characteristics and classified as alkaline feldspar granite. It contains 74–77 % microcline, 5–19 % quartz, 3–5 % plagioclase and 1–4 % "biotite" (Fig. 2c). In contrast, medium to fine-grained HYG indicates miarolitic texture and characterizes as alkali pluton. The granite is comprised of 59–66 % microcline, 21–35 % quartz, 3–6 % plagioclase and 0.5 % "biotite" (Fig. 2d). Likewise, the HMJ  $A_1$  intrusive body (30°56.26 N, 117°35.14 E) situated in the western part of the Luzong Basin is considered as

medium to coarse-grained pluton and classified as alkali granite based on mineralogical study. The rock comprises 81–83 % microcline, 5–12 % plagioclase and 11–13 % quartz (Fig. 2e). On the contrary, Luming granites exposed in Lesser Xing'an Range are mineralogically comprised of major constituents including 35–45 % K-feldspar, 5–10 % plagioclase, 25–35 % quartz and 3–8 % "biotite" with accessory phases such as zircon, apatite, and magnetite (Fig. 2f).

### 3. Geological background of Luming

The Luming porphyry Mo deposit is situated in SE (Fig. 3b), Lesser Xing'an Range of northeast (NE), China. NE China experienced two phases of progression in diverse tectonic environments. The Paleo-Asian Oceanic evolution initiated the collision of numerous blocks of microcontinents or terranes including Xing'an, Songliao, and Erguna from NW to SE during the Paleozoic and were alienated through chains of NE-trending faults (Fig. 3a). In the east, this area was represented through Paleo-Pacific Oceanic evolution and the Mongol-Okhotsk Ocean to NW during the Mesozoic which caused extensive magmatic activities and Jiamusi Massif accretion in NE, China (Wu et al., 2011). The occurrence of volcanic arcs and incorporation of terranes caused the evolution of the continental crust, as depicted through volcanic bodies and extensive granites in NE China. The Paleozoic igneous bodies are mainly dispersed in Great Xing'an and Zhangguangcai Range as well as North China Craton. These magmatic bodies are separated into Late Paleozoic and Early Paleozoic. Whereas, the Mesozoic igneous bodies can be alienated into three phases (Wu et al., 2011): (1) Late

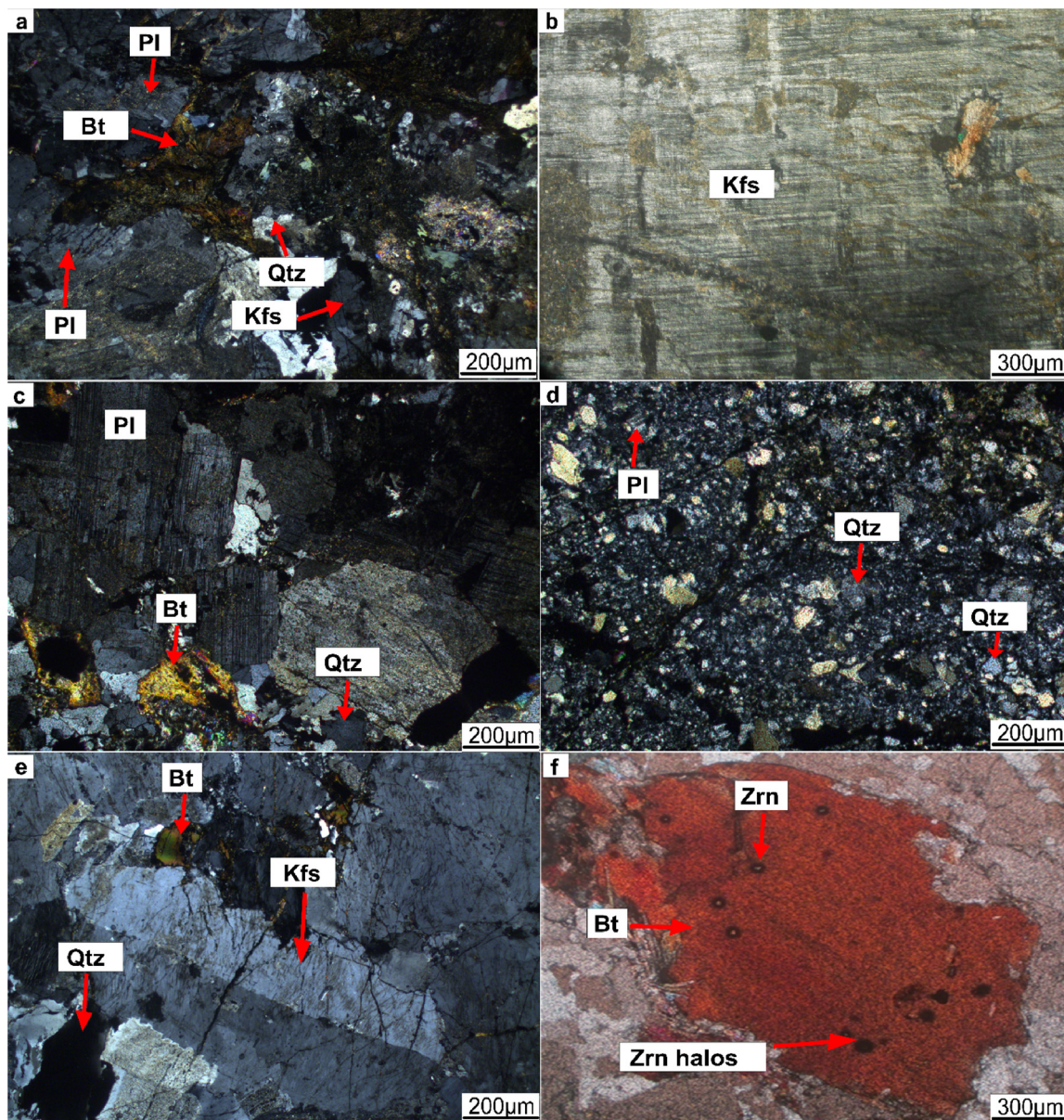


**Fig. 2.** Microphotographs of the LYRB and Luming granites under crossed-polarized light. (a) and (b) BSL and XSJ alkali-feldspar rich granites indicating Pl, Bt, Qtz and Kfs occurrence. (c) and (d) MT and HYG alkali granites showing presence of Bt, Pl and Qtz. (e) HMJ alkali granite presenting Bt, Kfs and strained Qtz. (f) Luming granite displaying Zrn dark halos and occurrence of Zrn as accessory phase in Bt. Mineral abbreviations: Pl = plagioclase, Qtz = quartz, Bt = "biotite", Kfs = potassium feldspar, Zrn = zircon.

Early Cretaceous–Late Cretaceous (133–88 Ma) (2) Late Jurassic–Early Cretaceous (150–138 Ma) and (3) Late Triassic–Middle Jurassic (228–160 Ma), which is principally exposed in eastern part of NE China particularly in the Lesser Xing'an Range and developed through the Paleo-Pacific Oceanic convergence. This range is situated in the eastern fragment of Central Asian Orogenic Belt (CAOB), which progressed from the incorporation of several microcontinental blocks between North China and Siberia Cratons (Jahn et al., 2009; Glorie et al., 2011). The eastern CAOB was subjected to intricate tectonic evolution in Paleozoic–Mesozoic, the termination of Paleo-Asian and Mongol–Okhotsk Oceans, and in Mesozoic–Cenozoic, the convergence of western Pacific Plate (Wu et al., 2001, 2007b; Zhang et al., 2012) which was responsible for producing extensive potential of mineralization in this region. From NW to SE, the eastern CAOB can be distributed into Xing'an, Songnen, Erguna, and Jiamusi Blocks, alienated through presence of numerous faults (F) namely Hegenshan–Heihe (F2), Tayuan–Xiguitu (F1), and Jiayin–Mudanjiang (F6) (Fig. 3a; Wu et al.,

2007a; Liu et al., 2014; Zeng et al., 2014). In Early Paleozoic, the Erguna Block attached to the Xing'an Block, however, the Jiamusi Block amalgamated with these multiple blocks during the Mesozoic (Ge et al., 2005; Wu et al., 2005). In the Late Paleozoic, Songnen Block fused with the composite blocks and Lesser Xing'an Range was interpreted as the NE portion of this block.

The rocks exposed in this Lesser Xing'an Range are represented by the presence of Cambrian, Ordovician, Permian and Cretaceous series including extrusive, terrigenous and carbonates (Fig. 3b; Shao et al., 2012). Sandstone, marble, and tuff are representative rocks of Cambrian however, extrusive and terrigenous bodies are indicative of Ordovician strata. Additionally, clastic rocks including sandstone, shale and metamorphic rock (marble) are present in Permian rocks and predominantly have experienced metamorphic actions (Shao et al., 2012; Yang et al., 2012). The Cretaceous rhyolitic volcanics, basaltic, trachy andesitic and tuff volcanic bodies are extensive in the entire range (Sun et al., 2013), while the volcanic rocks emerging around

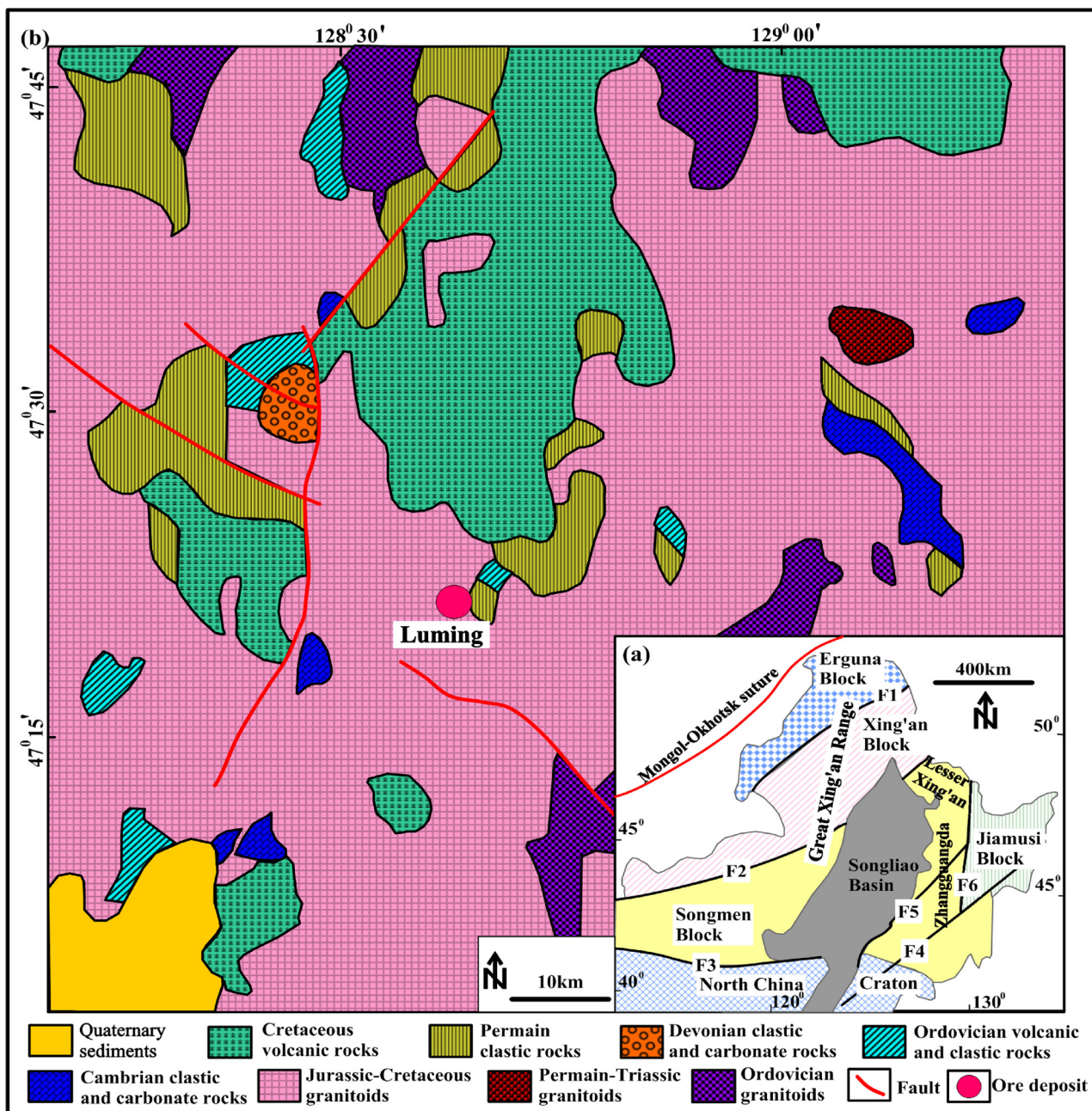


Fig. 3. (a) Tectonic map of NE China indicating various Ranges and Faults (F1-F6); (after Hu et al., 2014). (b) Geological map representing location of Luming area in Lesser Xing'an Range (modified from Hu et al., 2014).

Luming region are documented as rhyolites. The Lesser Xing'an Range predominantly contains Jurassic–Cretaceous granitoids with subordinate granites of Permian–Triassic, and Ordovician (Fig. 3b). These prime granitoids exist as batholiths as well as stocks and comprise chiefly of monzo–syeno granites and granite porphyries (Shao et al., 2012). The structural context is controlled by numerous faults which governed the dispersal of igneous bodies and mineralization varieties (Fig. 3a, b). A widespread mineralization including Pb–Zn and Mo, Fe are inherently linked with granitic rocks in this region (Chen et al., 2012; Shi et al., 2012; Yang et al., 2012). Several hydrothermal deposits emerged in NE China owing to extreme Paleozoic and Mesozoic magmatism. Specifically, massive and giant porphyry Mo deposits developed in the Luming area of NE China which makes it a vital place in China and worldwide (Chen et al., 2017; Qin et al., 2017).

The exposed granitic bodies in the deposits of Luming are chiefly granite porphyry and monzogranite (Fig. 4). The widely exposed

plutonic rocks in the mining area of Luming are mostly granite porphyry and monzogranites (Fig. 4a, b). The ore mineralization in these rocks reveals metasomatic textures and occur in the form of lens, bands, dissemination, veinlets as well as breccias and certain ore bodies are cut by a fault in the NWW trend (Fig. 4). Furthermore, extreme hydrothermal alteration and Mo mineralized zones are widespread around the granite porphyry. The potassic alteration is omnipresent and thoroughly linked with these potential mineralized zones. Based on alteration and mineralization attributes, the Luming monzogranite is an ore-bearing body and granite porphyry is considered as an ore-forming intrusion (Chen and Zhang, 2018). The zircon U–Pb ages of the granite porphyry and monzogranite are  $174 \pm 2$  Ma (Liu et al., 2014) and  $180.7 \pm 1.6$  Ma (Hu et al., 2014), respectively.

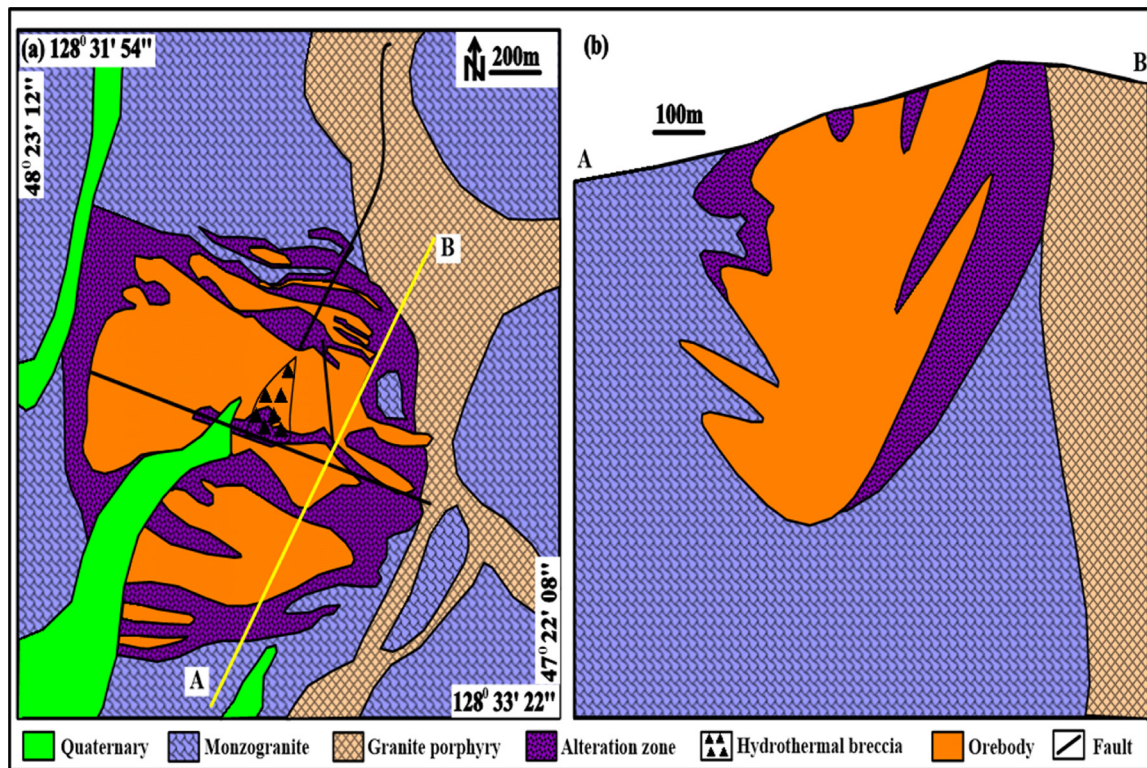


Fig. 4. a, b. Geological map of Luming deposit and its cross section of prospecting line (depth scale ranges 237.6 m – 693.3 m), (modified from Shao et al., 2012; Yang et al., 2012).

#### 4. Methodology

For this review of the apatite bearing granitic rocks of Luming and LYRB, representative fresh rock samples of granites were selected without obvious alteration. The same rock sample was distributed into two parts, the one was equipped for petrographic analysis of host rocks, the other was used to separate apatite. The petrographic analysis of the prepared slides was conducted by Leica polarizing microscopy. Apatite crystals were alienated from granitic rocks using standard heavy-liquid and magnetic methods, followed by hand-picking under the microscope. The selected apatite grains were then mounted in epoxy, and then polished. Polished blocks were examined analytically for apatites by four quadrants back scattered electron detector at the magnification of  $\times 500$ . Finally, cathodoluminescence (CL) images were photographed through 4 quadrants back-scattered detector operating at 20 kV accelerating voltage, a beam current of 20 nA, 1000 ms/step counting time and a working distance of 10 mm. These apatites were analyzed using the JSM-7800 thermal field Scanning Electron Microscope (SEM) connected with Energy Dispersive Spectrometer (EDS) in the State Key Laboratory of Ore Deposit Geochemistry (SKLODG), Institute of Geochemistry, Chinese Academy of Sciences. CL images of the analyzed apatites indicate that apatite grains have not been experienced hydrothermal alteration. Further, we searched the relevant published literature to compile geochemical data on major and trace elements of apatites with the target of debating their role in petrogenesis, mineralization, and geodynamic settings. We used two selection criteria while collecting the published geochemical data of apatites: (1) contents of apatite major elemental constituents were determined by electron microprobe (EMP), whereas amounts of apatite trace-elements were examined through laser ablation inductively coupled plasma–mass spectrometry (LA-ICP-MS).

Major elements in the apatite of LYRB were studied by JXA-8100 electron microprobe operated with wavelength-dispersive spectrometers at the State Key Laboratory of Mineral Deposits Research,

Nanjing University, China. The analyses were performed by using 10 nA, 15 keV, 10  $\mu\text{m}$  defocused electron beam. The standards used were norbergite for F,  $\text{Ba}_5(\text{PO}_4)_3\text{Cl}$  for Cl, and apatite for P and Ca analyses. Fluorine (F) and chlorine (Cl) were examined for 10 s in order to avoid volatile loss. Count times for other elements were 20 s. Also, F and Cl were measured by the  $K\alpha$  line on LDE1 crystal and PET crystal, respectively (Li et al., 2012a). Analytical accuracy for most of the elements is better than 1 %, however, for Cl and F precision is almost 5 %.

Minor and trace element contents in apatite were measured by LA-ICP-MS at the Key Laboratory of Mineralogy and Metallogeny, Guangzhou Institute of Geochemistry, Chinese Academy of Sciences. The Agilent 7500a ICP-MS instrument was connected to a Resonetics 193 nm ArF excimer laser ablation system. In situ LA-ICP-MS analyses of apatite were conducted on the same spot where electron microprobe studies were performed. The working conditions involved ablation frequency of 8 Hz, laser beam spot size of 43  $\mu\text{m}$ , and 80 mJ laser energy. The NIST SRM 610 was used as the external standard, while the Ca content, attained by an electron microprobe study, was employed as the internal standard. The NIST SRM 612 standard was used as a reference (Li et al., 2014). The analytical uncertainty is better than 10 % and the detection limit is less than 0.1 ppm for the analyzed apatite.

The major elemental analysis of the Luming apatite was conducted by a JEOL-JXA8100 electron microprobe operated with wavelength-dispersive spectrometry (WDS) at the Institute of Mineral Resources, Chinese Academy of Geological Sciences. The working conditions involved 10 nA beam current and 15 kV accelerating voltage. To distinguish the specific X-ray patterns, twenty seconds (s) of counting time were selected for most elements, while 10 s was taken for P and Ca and 40 s was selected for F.

The trace-element compositions were measured by LA-ICP-MS at the State Key Laboratory of Geological Processes and Mineral Resources, China University of Geosciences (Wuhan). The working conditions are the same as those demonstrated by Liu et al. (2008). Laser sampling was executed by the GeolasPro laser ablation system that comprised of

COMPexPro 102 ArF excimer laser (with maximum energy of 200 mJ and wavelength of 193 nm) and a MicroLas optical system. An Agilent 7700e ICP-MS instrument was used to obtain ion-signal intensities. The frequency of the laser and spot size was fixed to 60 mm and 44 mm, respectively. For the determination of trace-elements, Ca was used as the internal standard. According to the EPMA, the Ca content in the apatites was used as an internal standard to correct matrix effects, signal drift, and differences in the ablation yield between samples and reference materials. Moreover, for the in situ apatite analysis, BIR-1 G, BCR-2 G, and BHVO-2 G were used as external standards (Liu et al., 2008). Each analysis incorporated a background acquisition of almost 20–30 s followed by 50 s of data acquisition from the sample. An Excel-based software program, ICPMSDataCal, was used to perform the off-line selection and combination of background and examined signals, time-drift corrections and quantitative calibration for trace-element study (Liu et al., 2008).

## 5. Geochemical characteristics of apatites from Luming and LYRB

### 5.1. Major and trace element compositions of apatite

Variations observed in the apatite chemical compositions are presented in Tables 1–4. The major constituents of apatite from LYRB and Luming (LM) comprise SiO<sub>2</sub>, CaO, P<sub>2</sub>O<sub>5</sub>, MnO, FeO, Cl, and F.

The SiO<sub>2</sub> contents of apatite from LYRB A-type granites (0.09–1.69 wt.%, average 0.48 wt.%) are significantly higher in comparison to those of apatite from Luming granites (0–0.55 wt.%, average 0.15 wt.%). Apatite from LYRB reveals comparatively lower concentrations of CaO (51.67–54.66 wt.%, average 53.80 wt.%), however, the apatites from Luming have greater contents (53.91–55.23 wt.%, average 54.48 wt.%). Meanwhile, LYRB and Luming apatites have P<sub>2</sub>O<sub>5</sub> concentrations in the range of (39.83–43.33 wt.%, average 41.91 wt.%) and (42.26–43.36 wt.%, average 42.63 wt.%) respectively. The amounts of MnO in apatite from LYRB (0.06–0.75 wt.%, average 0.28 wt.%) are considerably higher in contrast to apatite from Luming

(0.03–0.09 wt.%, average 0.05 wt.%). Apart from these, the FeO quantities in apatite from LYRB (0.02–0.23 wt.%, average 0.09 wt.%) are fairly greater in comparison to apatite from Luming (0–0.05 wt.%, average 0.03 wt.%). As for halogens, apatites in LYRB typically exhibit higher Cl (0.02–1.45 wt.%, average 0.35 wt.%) and lower F contents (1.51–3.85 wt.%, average 2.35 wt.%) comparative to apatites from Luming which represent highest F (3.36–5.29 wt.%, average 3.99 wt.%) and the lowest Cl concentrations (0–0.04 wt.%, average 0.02 wt.%).

The apatites from Luming express a range of Th (3.6–34 ppm, average 13 ppm) and U (2.7–38 ppm, average 9.4 ppm), however, LYRB apatites indicate lack of both Th and U contents. Likewise, the Sr concentrations from LYRB have a wide range (18.7–457 ppm, average 171.74 ppm) and narrow range (146–187 ppm, average, 164.5 ppm) for Luming. Meanwhile, Y concentration is lower in apatites from LYRB (717–7175 ppm, average 1993 ppm) than that of Luming (1267–3423 ppm, 2123 ppm). The calculated  $\delta\text{Ce}$  and  $\delta\text{Eu}$  values in LYRB are (0.96–1.12, average 1.02) and (0.04–0.43, average 0.21), however, (0.98–1.09, average 1.04) and (0.12–0.23, average 0.16) for Luming. The  $\Sigma\text{LREE}/\Sigma\text{HREE}$  ratios in apatite grains of LYRB and Luming exhibit range of (1.0–7.6, average 5.19) and (0.58–7.6, average 1.2) respectively. Both varieties of apatites are enriched in light rare earth elements (LREEs) compared with heavy rare earth elements (HREEs) and exhibit strong negative europium (Eu) anomalies. Despite the REEs distribution patterns, the combination of (La/Sm)<sub>N</sub> and (Yb/Sm)<sub>N</sub> in apatites of Luming and Lower Yangtze exhibit positive correlation. Further, the apatites (La/Yb)<sub>N</sub> and Eu/Eu\* ratios in LYRB and Luming indicate higher variations.

### 5.2. Apatite REEs, Sr, SiO<sub>2</sub> and MnO contents as indicators of petrogenesis

Europium (Eu) anomaly in apatite is associated with the competition between plagioclase and apatite in a melt. Earlier crystallization of abundant plagioclase than the apatite crystallization will produce a magma depleted in Eu, signifying that late crystallized apatites will have considerably negative europium (Eu) anomalies. Nevertheless,

**Table 1**

Major and minor elements (wt.%) of apatite from the Early Cretaceous A-type granites of the LYRB (Jiang et al., 2018a).

Sample No	CaO	P <sub>2</sub> O <sub>5</sub>	MnO	SiO <sub>2</sub>	FeO	SrO	MgO	F	Cl	Total
BSL9-01	52.33	41.53	0.75	0.31	0.23	0.01	0.09	1.51	1.45	98.21
BSL9-02	53.86	41.57	0.37	0.31	0.1	–	0.05	1.7	1.21	99.17
BSL9-03	53.36	41.88	0.2	0.4	0.08	0.01	0.04	1.57	1.26	98.8
BSL9-04	54.14	40.76	0.23	0.34	0.08	–	0.05	1.76	1.21	98.57
BSL9-05	53.33	42.23	0.37	0.26	0.17	0.01	0.01	1.75	0.95	99.08
HMJ2-03	53.42	42.11	0.2	0.5	0.06	–	–	2.31	0.04	98.64
HMJ2-05	51.67	39.83	0.12	1.69	0.11	0.02	0	2.2	0.04	95.68
HMJ2-06	53.73	41.77	0.17	0.73	0.14	0.01	0.05	2.97	0.04	99.61
HMJ2-07	53.59	41.48	0.17	0.48	0.11	0.01	0.01	2.39	0.04	98.28
HMJ2-08	54.04	41.34	0.07	0.62	–	0.01	–	2.2	0.03	98.31
HYG3-01	54.35	42.88	0.13	0.09	0.14	–	0.06	1.86	0.95	100.46
HYG3-02	53.76	42.54	0.41	0.44	0.04	0.02	0.02	2.55	0.03	99.81
HYG3-03	53.62	41.19	0.49	0.93	0.05	0.01	0	2.63	0.02	98.94
HYG3-04	54.16	43.33	0.06	0.12	0.13	0.01	0.08	2.06	1.02	100.97
HYG3-06	54.13	41.81	0.29	0.64	0.11	0	0.02	2.43	0.02	99.45
XSJ9-01	54.4	41.89	0.45	0.36	–	0.01	0.02	2.51	0.1	99.74
XSJ9-02	53.93	41.46	0.41	0.46	0.03	0.01	0.02	2.28	0.09	98.69
XSJ9-03	53.93	41.64	0.3	0.28	0.09	0.01	0.02	2.1	0.11	98.48
XSJ9-04	53.85	41.35	0.46	0.39	0.02	–	0.01	2.22	0.09	98.39
XSJ9-05	54.53	42.23	0.31	0.25	0.04	0.03	0.02	2.08	0.05	99.54
MT12-01	54.25	42.62	0.15	0.31	0.11	–	0.04	2.48	0.05	100.01
MT12-02	54.23	42.25	0.17	0.53	0.16	–	0.06	2.39	0.08	99.87
MT12-03	54.32	42.74	0.23	0.24	0.15	0.03	0.04	2.42	0.07	100.24
MT12-04	54	42.48	0.17	0.3	0.05	0.02	0.05	2.48	0.07	99.62
MT12-06	54.66	42.76	0.07	0.41	0.1	0.03	0.03	2.4	0.06	100.52
HYG1-01	54.22	42.5	0.29	0.6	0.04	0.01	0.01	2.38	0.03	100.08
HYG1-02	53.85	41.82	0.26	0.39	0.02	0.01	0.02	2.5	0.01	98.88
HYG1-03	54.14	42.04	0.25	0.27	0.09	–	0.04	2.61	0.01	99.45
HYG1-04	53.61	41.8	0.36	0.77	0.05	0.01	0.02	2.36	0.05	99.03
HYG1-05	54.06	42.19	0.29	0.43	–	–	0.02	2.62	0.02	99.63

**Table 2**

Trace elements (ppm) of apatite from the Early Cretaceous A-type granites of the LYRB (Jiang et al., 2018a).

Sample No	La	Ce	Pr	Nd	Sm	Eu	Gd	Tb	Dy	Ho	Er	Tm	Yb	Lu	V	Sr	Y	δCe	δEu
BSL9-01	1813	4555	566	2349	472	24.8	401	56.1	326	65.8	174	24.4	152	21.3	14.1	202	1912	1.07	0.17
BSL9-02	1837	5067	643	2714	561	26.7	472	66.8	386	76.4	203	28	177	24.1	13.6	163	2206	1.12	0.15
BSL9-03	3250	6968	786	3100	535	37.3	418	53.9	300	58.2	155	21.4	135	18	19.5	326	1581	1.01	0.23
BSL9-04	2520	5419	621	2555	444	47.3	355	43.3	231	44.1	105	13.1	74.4	10.2	23.9	400	1149	1.01	0.35
BSL9-05	1477	4253	560	2398	526	32	455	65.6	380	76.1	204	29.5	195	26.7	10.2	238	2175	1.12	0.19
HMJ2-03	4829	10661	1265	5119	870	16.8	636	73.6	361	61.2	140	16.9	93	11.6	6.57	54.9	1763	1.01	0.06
HMJ2-05	4282	11693	1582	7182	1768	28.1	1593	233	1329	254	652	91.4	538	62.2	0.53	130	7175	1.08	0.05
HMJ2-06	3725	8320	1022	4215	757	33	589	67.5	337	58.6	134	16.6	94.1	12.2	6.5	152	1648	1.00	0.14
HMJ2-07	4526	10322	1239	5197	908	27.1	711	77.3	377	66	145	17.5	93.4	12.4	5.98	55.1	1746	1.03	0.09
HMJ2-08	3009	7582	933	3871	840	12.8	760	106	599	115	292	39.3	230	30.6	0.12	198	3417	1.08	0.04
HYG3-01	2298	4890	551	2213	376	19.2	276	33.9	180	32.7	81	10.4	62.2	8.1	28.6	260	920	1.01	0.17
HYG3-02	2575	4411	366	1133	146	12.3	127	16.9	108	23.8	73.9	11.3	77.2	11.7	24.7	102	849	0.96	0.27
HYG3-03	4181	8978	951	3536	592	32.9	527	74.6	448	91.1	246	32.2	194	25.5	8.09	18.7	2653	1.04	0.17
HYG3-04	2262	4688	515	2050	339	16.9	245	28.9	150	26.6	64.1	8.09	48.7	6.18	22.5	213	717	1.00	0.17
HYG3-06	4045	8177	740	2373	349	15	317	48.5	325	72.6	212	29.8	187	25	3.71	40.1	2374	1.05	0.13
XSJ9-01	3856	7427	722	2560	377	16.1	325	41.7	238	51.4	149	19.3	126	18.9	17.4	237	1623	1.00	0.13
XSJ9-02	3722	7357	728	2670	406	17	344	44.6	261	56.2	160	21.3	133	19.5	20.6	291	1791	1.01	0.13
XSJ9-03	2787	5567	585	2384	371	18.2	276	32.1	169	33.7	92.4	12.2	79.6	12	38.7	204	1043	0.99	0.16
XSJ9-04	2798	5950	670	2794	450	35.9	331	40.5	209	40.5	103	13.2	79.5	11.2	21.8	107	1180	1.01	0.27
XSJ9-05	2723	5173	506	1859	311	11.2	288	36.3	199	41.9	114	14.4	85.6	12.8	26.1	159	1250	0.99	0.11
MT12-01	2305	5165	621	2542	468	51.5	378	49.6	269	49.1	124	15.3	82.5	10.9	27.7	174	1327	1.02	0.36
MT12-02	3009	6915	852	3563	667	89.1	552	72.4	401	75.1	183	23	128	17.1	15.6	457	1977	1.02	0.43
MT12-03	2293	5211	623	2578	475	48	385	49.5	271	51.1	123	14.7	82.1	10.7	30.9	168	1350	1.03	0.33
MT12-04	2288	5110	612	2525	470	53.6	378	49.3	264	50.2	122	15.2	81.4	10.9	22.8	243	1339	1.02	0.37
MT12-06	2754	5497	606	2464	447	52.9	371	48.2	262	50.8	123	16.2	89.6	12.6	15.6	251	1350	0.98	0.38
HYG1-01	4349	7738	658	1999	263	18.6	223	33	222	52.6	165	25.1	172	24.5	6.89	53.3	1876	0.98	0.22
HYG1-02	4378	7706	638	1936	240	19.7	189	25.6	158	37.2	113	17.7	122	18	6.7	86.7	1314	0.98	0.27
HYG1-03	2608	4654	421	1447	204	16.7	172	21.6	124	26.8	74.9	10.7	69.3	10.2	23.7	99.8	847	0.97	0.26
HYG1-04	4856	9789	962	3241	545	22.1	552	84.4	529	115	306	39.5	236	31.5	3.75	67.8	3300	1.02	0.12
HYG1-05	4166	7692	685	2096	285	17.5	258	38.2	252	61.1	185	27.2	176	25.4	8.26	48.3	2032	0.99	0.19

crystallization of apatite before the start of plagioclase crystallization would be free of these anomalies (Tollari et al., 2008). The critical understanding of Eu mainly its negative anomaly (Drake, 1975), specifies that the crystallization of plagioclase decreases europium in the melt, prompting and producing minor quantities of europium in apatite. Therefore, the noticeable strong negative europium (Eu) anomalies in the Lumming and Lower Yangtze apatite is inducing from plagioclase crystallization earlier than apatite. This interpretation is parallel with the conclusions of Azadbakht et al., 2018. Moreover, all the studied

apatites in Lumming granites and A-type granites of Lower Yangtze (BSL, XSJ, MT, HYG, HMJ) plot in the field of magmatic apatite in SiO<sub>2</sub>-MnO diagram deducing that the apatite grains have not subjected to perceptible alteration (Fig. 5); hence, apatites composition reflects the actual attributes of parental melt. The apatites in the granites of Lumming reveal the common occurrence of idiomorphic crystals as well as the presence of phenocrysts, whereas, apatites from Lower Yangtze granites (BSL, XSJ, MT, HYG, HMJ) also exhibit well-developed crystals (Fig. 6). These textural characteristics of apatites from both granites deduce that

**Table 3**

Major and minor oxides (wt.%) of apatites from Lumming granites (Chen and Zhang, 2018).

Sample No	CaO	P <sub>2</sub> O <sub>5</sub>	MnO	SiO <sub>2</sub>	FeO	Al <sub>2</sub> O <sub>3</sub>	MgO	Na <sub>2</sub> O	K <sub>2</sub> O	TiO <sub>2</sub>	BaO	SO <sub>3</sub>	F	Cl	Total	
LM-1	55.23	42.39	0.03	0.15	-	-	-	0.02	-	-	-	0.05	3.39	-	101.26	
LM-2	54.63	42.27	0.05	0.17	-	-	0.02	-	-	-	-	0	3.85	-	100.99	
LM-3	54.35	42.7	-	0.12	-	-	-	-	-	0.07	0.02	0.06	3.69	0.02	101.03	
LM-4	54.3	42.49	-	0.22	-	-	-	-	-	-	-	0.05	3.63	-	100.69	
LM-5	54.31	43	0.05	0.17	-	-	0	-	-	-	0.02	0.07	3.64	0.03	101.29	
LM-6	54.02	42.98	0.05	0.15	-	-	0.03	-	-	-	-	0.02	3.62	-	100.87	
LM-7	54.18	42.44	0.06	0.19	0.03	0.02	-	0.04	-	-	-	0.06	3.36	-	100.38	
LM-8	54.41	42.78	0.08	0.18	0.03	-	-	0.03	-	-	-	0.02	3.65	-	101.18	
LM-9	54.6	42.3	-	0.09	-	-	-	-	-	-	-	0.05	0.07	3.82	-	100.93
LM-10	54.51	42.29	0.06	0.14	-	-	-	-	-	0.1	-	-	4.9	0.02	102.02	
LM-11	55.02	42.62	0.03	0.14	0.04	-	-	0.05	-	0.06	-	0.04	3.52	0.03	101.55	
LM-12	54.94	42.77	-	0.08	0	0.02	-	-	-	-	-	0.02	3.58	0.04	101.45	
LM-13	54.59	42.33	0.03	0.13	0.05	-	-	-	-	-	-	0.08	5.23	-	102.44	
LM-14	54.4	42.88	0.06	0.09	-	-	-	-	-	-	-	0	4.69	0.02	102.14	
LM-15	54.85	42.41	0.09	0.04	0.05	-	-	-	0.01	0.08	-	0.03	3.57	0	101.13	
LM-16	53.91	42.3	0.04	0.55	-	-	-	-	-	-	-	0.06	3.65	-	100.51	
LM-17	54.24	42.26	0.09	0.2	0.03	-	-	-	-	-	-	0.04	5.29	0.03	102.18	
LM-18	54.36	42.34	-	0.15	-	-	-	-	-	0.07	-	0.02	3.78	0.02	100.74	
LM-19	54.15	43.09	0.05	0.06	-	-	-	-	-	-	-	0.06	4.27	-	101.68	
LM-20	54.55	43.36	0.04	0	-	-	0.03	0.03	-	-	-	0.05	3.59	-	101.65	
LM-21	55.12	42.34	0.04	0.06	-	-	0	0	-	-	-	0	4.84	-	102.4	
LM-22	53.91	42.74	0.09	0.24	-	-	0.06	0.06	0.01	-	-	0.04	3.82	-	100.97	
LM-23	54.55	42.92	0.03	0	-	-	-	-	0.01	0.05	0.02	0.05	3.75	-	101.38	
LM-24	54.48	43.1	0.05	0.16	0.03	0.04	-	-	-	-	-	-	3.54	0.02	101.42	
LM-25	54.26	42.54	-	0.23	-	-	-	-	-	-	-	-	3.91	-	100.94	

**Table 4**  
Trace elements (ppm) of apatites from Luming granites (Chen and Zhang, 2018).

Sample No	La	Ce	Pr	Nd	Sm	Eu	Gd	Tb	Dy	Ho	Er	Tm	Yb	Lu	Ga	Y	Li	Ge	Th	U	Sr	δCe	δEu
LM-1	465	1447	230	1107	343	14.9	378	55.1	347	72.7	202	34.5	192	26.1	27.7	2144	0.16	9.86	11.9	4.98	150	1.05	0.12
LM-2	542	1722	274	1379	468	21.1	557	86.8	558	123	328	54.8	309	43.8	32.7	3423	0.17	13.3	34	38	146	1.06	0.12
LM-3	278	689	101	519	204	15.4	270	43.1	276	58.7	154	24.6	129	19	12.5	1546	0.52	4.74	6.48	5.4	168	0.98	0.20
LM-4	273	926	154	768	279	19.2	341	55.7	346	73.6	191	32.1	182	25.8	17.6	2075	0.32	7.51	9.37	6.76	173	1.06	0.19
LM-5	356	1093	177	912	324	17.7	424	68.5	444	95.5	251	41.6	226	32.4	20	2671	0.25	8.13	17.5	7.32	174	1.04	0.14
LM-6	528	1590	237	1179	367	18.3	411	61.4	388	82.7	222	37.3	205	31.2	28	2366	0.11	9.42	15.8	8.3	149	1.07	0.14
LM-7	225	905	189	1170	507	24.2	610	95.5	566	113	273	42.2	213	28.6	19.5	3102	0.5	10.7	11.2	6.48	162	0.98	0.13
LM-8	292	1010	174	930	360	19.1	454	74.9	494	105	279	46.8	263	36.7	18.6	2993	0.46	8.52	13.6	7.55	174	1.05	0.14
LM-9	469	1210	170	842	255	16.3	300	44.3	276	59.2	161	26.5	144	21.4	19.7	1738	0.15	7.36	17.4	12.2	182	1.03	0.17
LM-10	477	1539	237	1163	335	15.8	353	51.1	316	69.7	191	32.5	184	25.6	25	2063	0.19	11	12.8	7.48	152	1.09	0.13
LM-11	225	933	192	1147	482	28.6	557	85.3	521	101	254	40.5	230	30.2	17.4	2780	0.45	9.27	7.35	3.59	179	1.00	0.16
LM-12	426	1319	201	1005	312	17.4	351	53	334	72.2	194	33.2	188	27.6	20.8	2076	0.2	7.72	12.8	6.44	154	1.08	0.16
LM-13	248	801	123	612	197	11.4	254	36.4	228	48.9	123	17.8	89.1	13.4	12.9	1314	0.51	5.17	6.04	3.68	162	1.09	0.15
LM-14	255	881	149	785	288	15.6	363	56.7	356	75.6	196	30.9	160	22.5	14.9	2080	0.36	6.66	9.28	5.59	165	1.06	0.14
LM-15	336	1011	156	772	217	12.8	244	35	215	45.9	124	20.5	114	16.6	16.6	1349	0.21	6.73	6.64	3.08	160	1.05	0.16
LM-16	434	1064	145	692	227	17.3	295	46.1	292	64.2	169	26.9	148	22.1	15.3	1725	0.28	5.57	18.9	16.6	167	1.01	0.20
LM-17	309	987	163	857	277	24.2	349	53.2	335	73.9	200	35.5	198	29.1	16	2218	0.19	6.86	13.3	8.92	187	1.04	0.23
LM-18	399	1045	146	683	233	13.5	314	46.9	286	58.3	145	21.6	112	16.8	14.8	1473	0.24	5.32	6.28	4.69	159	1.04	0.15
LM-19	466	1506	238	1182	317	15.9	335	45.8	265	54.7	142	22.8	132	18.7	22.5	1614	0.64	9.52	15.5	6.75	159	1.07	0.14
LM-20	322	807	117	566	199	10.3	252	38	227	47.3	121	19	98.5	14.4	11.9	1267	1.78	4.57	3.62	2.73	164	0.99	0.14

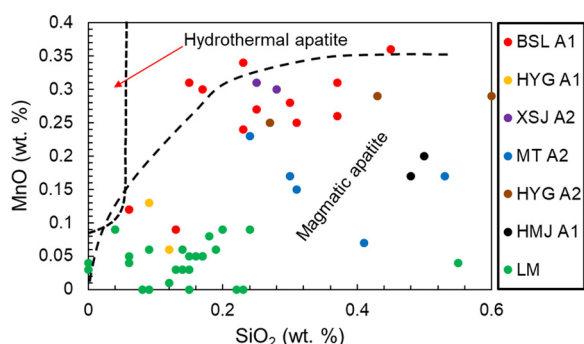


**Fig. 5.** Plot of SiO<sub>2</sub> (wt.%) vs MnO (wt.%) for apatites hosted in Luming (LM) and LYRB granites (BSL, XSJ, MT, HYG, HMJ). The fields are after Chen et al. (2017).

the apatites crystallized at earlier stage during crystallization. Therefore, the noticed concentrations of major and trace elements in both apatites were principally governed by their contents in parental melts and partitioning between apatite/melt or competing minerals.

The apatite composition specifically REEs patterns/ratios, Sr contents, and Eu anomalies deliver strong evidence for geochemical processes in silicic magmas. Several researches have confirmed that differences in apatite trace elements are associated to the magma varieties, geological settings, crystallization history, and impacts of other minerals (Belousova et al., 2002; Chu et al., 2009; Miles et al., 2013; Zirner et al., 2015). Two chondrite-normalized REEs patterns are present in the apatite from Lower Yangtze and Luming respectively, and both sets of apatites reveal comparable chondrite-normalized REEs patterns, however, HREEs contents of Luming is higher comparative to Lower Yangtze (Fig. 7a,b). Apatite grains from Lower Yangtze have

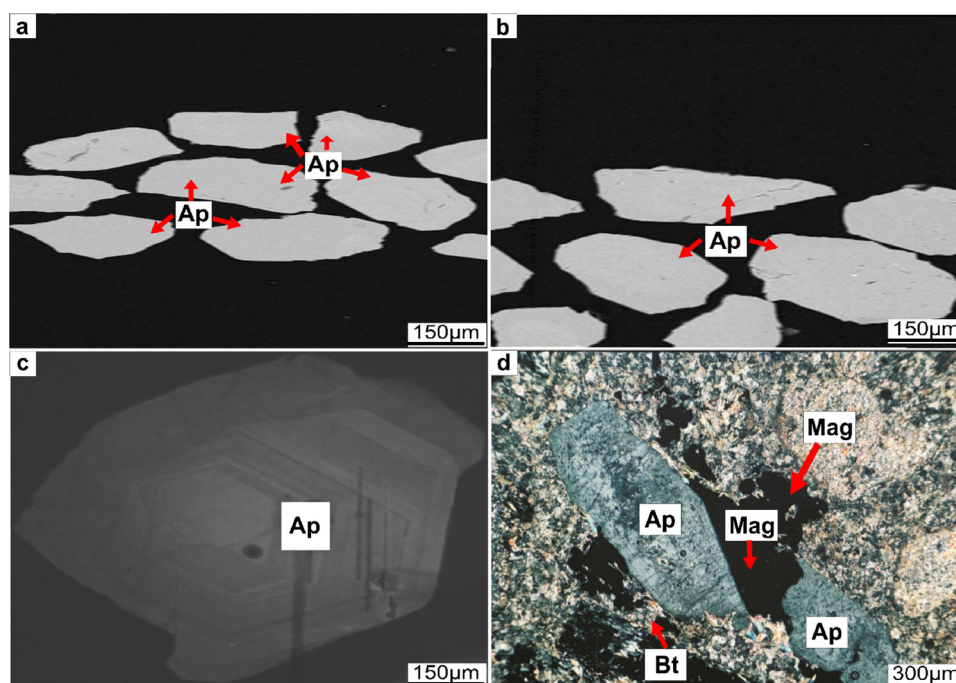


**Fig. 6.** CL images of the apatites from the granites of LYRB. (a-c) Presence of phenocrysts and idiomorphic crystal of apatite. (d) Microphotograph indicating well-developed apatite phenocrysts and occurrence of magnetite and "biotite" in the granitic body of Luming. Abbreviations: Ap-apatite; Mag-magnetite; Bt-"biotite".

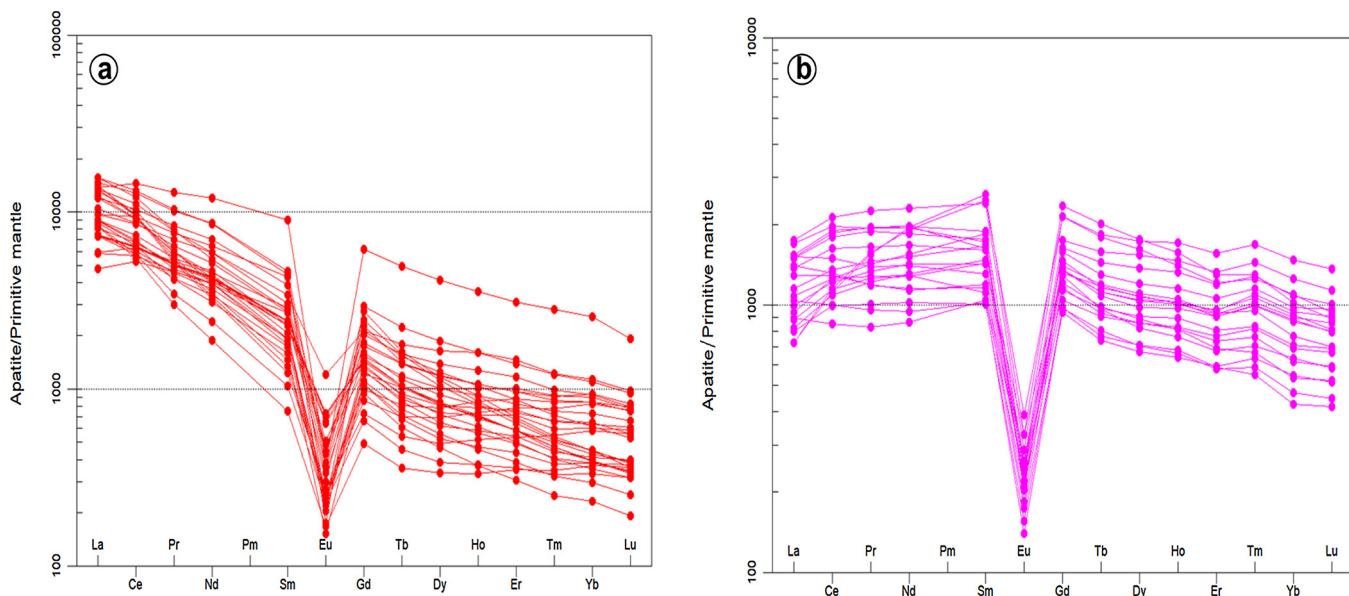


Fig. 7. a, b. Primitive mantle normalized rare earth elements (REEs) diagrams for apatites of LYRB and Luming plutons indicating strong negative Eu anomalies respectively (Boynnton, 1984).

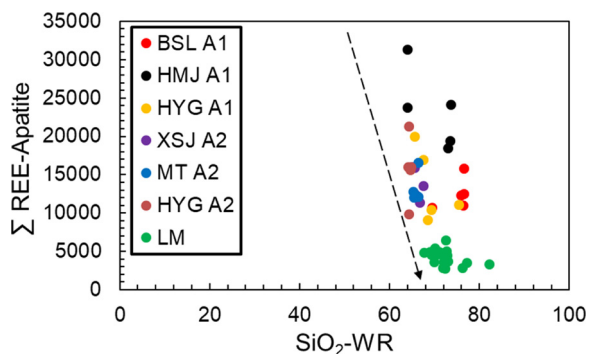


Fig. 8. Apatite  $\Sigma$ REE concentrations of LYRB and Luming vs whole rock  $\text{SiO}_2$  contents.

higher concentrations of  $\Sigma$ REE (4914.3–31287.7 ppm, average 14737.4 ppm) in comparison to apatite grains from Luming (2780.8–6466.5 ppm, average 4233.2 ppm). [Prowatke and Klemme \(2006\)](#) presented that apatite crystallizing in silicic systems can host up to approximately an order of magnitude more REEs comparative to apatite from mafic schemes. As displayed in [Fig. 8](#), all of the studied apatites from Lower Yangtze (BSL, XSJ, MT, HYG, HMJ) and Luming together confirm that the REE concentrations indicate variation with the whole rocks  $\text{SiO}_2$  contents (the calculated data for whole rock  $\text{SiO}_2$  content in Yangtze granites are from [Yang et al., 2017](#); [Jiang et al., 2018b](#) whereas, Luming granites  $\text{SiO}_2$  contents are from [Hu et al., 2014](#) and [Liu et al., 2014](#)). The  $\Sigma$ REE concentrations of apatite reduce consecutively from Lower Yangtze to Luming, implying that the  $\Sigma$ REE concentrations in apatites are principally governed by the  $\text{SiO}_2$  in the melt ([Fig. 8](#)).

The apatite grains from Lower Yangtze Belt show right inclined REE pattern, HREE-depleted, enriched in LREE and have noteworthy strong negative Eu anomaly on the REEs plots ([Fig. 7a](#)). However, apatite grains from Luming granites are represented by the presence of LREE enrichment patterns, with relatively flat REE distribution and indicate a strong negative Eu anomaly ([Fig. 7b](#)). The  $\Sigma$ LREE/ $\Sigma$ HREE ratios in apatite grains of the Yangtze belt range from 1.0–7.6 (average, 5.19). In contrast, the apatite grains of Luming reveal range of these ratios 0.58–7.6 (average, 1.2). The variations in trace element compositions in Lower Yangtze and Luming apatite may impart minerals, for instance,

allanite, monazite, hornblende, zircon, titanite, xenotime, and feldspar which compete for the REE in the evolved magmas when apatite develops ([Bea, 1996](#); [Hoskin et al., 2000](#); [Miles et al., 2013](#)). Therefore, the trace elements in apatite grains of Lower Yangtze are mainly governed by titanite crystallization ([Fig. 9](#)). It also designates that the zircon crystallization in Lower Yangtze granites was affected by the apatite and titanite crystallization as well ([Fig. 8](#)). This finding is consistent with [Xie et al., 2018](#). The apatite normalized REE patterns from Lower Yangtze Belt confirm significant LREE enrichment ( $\Sigma$ LREE/ $\Sigma$ HREE = 1.0–7.6, average 5.19) relative to Luming apatite. This consideration can propose that titanite crystallized earlier than apatite in Lower Yangtze since titanite is famous to hold the HREEs ([Hoskin et al., 2000](#); [Miles et al., 2013](#)). In contrast, the lower  $\Sigma$ LREE/ $\Sigma$ HREE values (0.58–7.6, average 1.2) in Luming apatite, suggests that titanite crystallization did not take place earlier to or at the equivalent time as apatite. The trace elements in Luming are predominantly controlled via crystal fractionation/crystallization of apatite ([Fig. 9](#)).

Experiments have confirmed that the apatite/melt partition coefficients for MREEs are higher relative to LREEs and HREEs ([Fujimaki, 1986](#); [Watson and Green, 1981](#)) which triggers the  $(\text{La}/\text{Sm})_N$  values to be lower in apatite grains comparative to the melt. In this study of Luming apatite, the  $(\text{La}/\text{Sm})_N$  values of the apatites (0.28–1.2) are lower than those of the Luming granites (2.71–7.57, the calculated values are from [Liu et al., 2014](#)), which is parallel with the

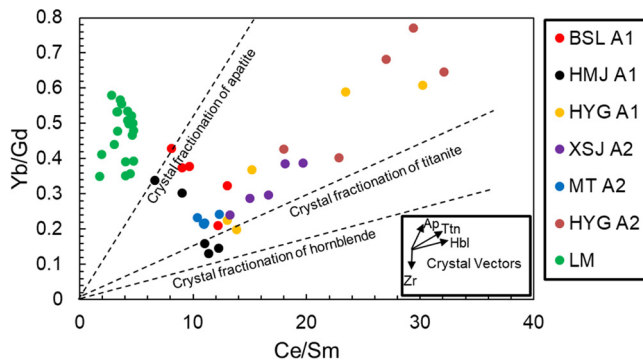


Fig. 9. Binary plot of apatite Yb/Gd and Ce/Sm ratios for plutons of LYRB (BSL, XSJ, MT, HYG, HMJ) and Luming (LM). Vectors indicate hornblende (Hbl), titanite (Ttn), apatite (Ap) and zircon (Zr) crystal fractionation.

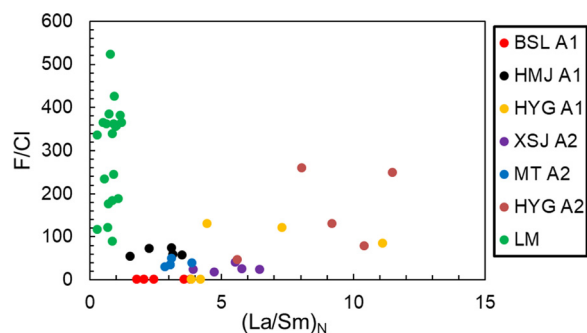


Fig. 10. Plot of  $(La/Sm)_N$  with F/Cl indicating higher F/Cl in Luming samples and higher  $(La/Sm)_N$  in LYRB granites (BSL, XSJ, MT, HYG, HMJ).

experimental results. However, apatite grains from Lower Yangtze have  $(La/Sm)_N$  ratios (0.85–11.47) which are greater relative to the host rock (3.9–4.9; the data for whole rock is calculated from Jiang et al., 2018a,b). Hence, the whole-rock rare earth element (REE) composition may signify the REE composition of the magma. Apatite grains from Luming have greater F/Cl ratios in comparison to Lower Yangtze (Fig. 10). Prior researches have presented that the exsolution of Cl-bearing hydrothermal stages can eliminate more LREEs relative to MREEs and HREEs from the magma. Consequently, the crystallized apatite grains from the melt after Cl-bearing fluid exsolution will have greater F/Cl; however, inferior  $(La/Sm)_N$  values. Apatite grains of the Luming is also crystallized from the melt after the exsolution of Cl-bearing fluid, therefore, they comprise higher F/Cl but lower  $(La/Sm)_N$  values (Fig. 10) which is consistent with observations of Flynn and Burnham, 1978; Keppler, 1996. We propose that the apatite grains from Luming with higher F/Cl may attain this greater ratio from higher F/Cl melts, while the higher  $(La/Sm)_N$  values in Lower Yangtze apatite grains (Fig. 10) are principally governed via titanite that developed before apatite (Hoskin et al., 2000; Miles et al., 2013).

The apatite Sr concentrations reveal a positive correlation with  $SiO_2$  contents of host rocks (Fig. 11). Chu et al. (2009) demonstrated that apatite generally comprises less Sr concentrations relative to host-rock. Apatite grains from Luming exhibit contents of Sr in the range of (146–187 ppm, average 164.5 ppm) which is less comparative to whole rock (105–587 ppm, average 290.43 ppm; the calculated values are from Liu et al., 2014). Conversely, the amounts of Sr in apatite grains of Lower Yangtze (18.7–457 ppm, average 171.74 ppm) are much greater in contrast to host rock (4.81–46.1 ppm, average 22.39 ppm; the data for whole rock is calculated from Jiang et al., 2018b). Hence, the apatite diverse Sr contents are not wholly measured by melt composition. Chu et al. (2009) presented that the apatite Sr concentrations are associated with the degree of differentiation and compositional

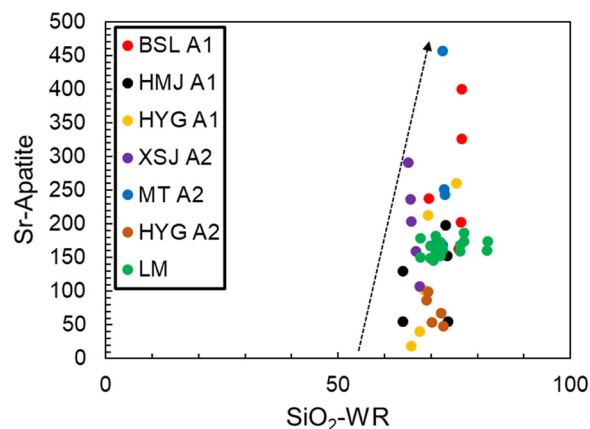


Fig. 11. Positive correlation of apatite Sr contents with whole-rocks  $SiO_2$  contents.

variation in the melt source region. Belousova et al. (2001) also exhibited that the apatite amounts of Sr indicate consistent variation with the host rock. Higher contents of Sr in apatite grains from Lower Yangtze than the whole rock might indicate restricted feldspar crystallization since feldspars favourably hold Sr (Aigner-Torres et al., 2007) or notable mafic magmatic involvement from mantle sources (Sha and Chappell, 1999; Chu et al., 2009). Consequently, the magma origin of Lower Yangtze apatite may incorporate more mafic magma in contrast to Luming apatite.

### 5.3. Apatite Ce, Eu and Mn contents as pointer of the redox state of parental magma

The redox state of magma can be described and assessed by the occurrence of particular elements in apatite framework such as Mn, Ce, Eu and S (Pan et al., 2016). The apatite Eu and Ce anomalies are significant as proxies to determine the redox state of magma (Cao et al., 2012; Miles et al., 2014). Two ionic valences are revealed by Eu and Ce which are  $Eu^{3+}/Eu^{2+}$  and  $Ce^{4+}/Ce^{3+}$  respectively. The  $Eu^{3+}$  indicates a more equivalent ionic radius with  $Ca^{2+}$  comparative to  $Eu^{2+}$ .  $Ce^{3+}$  exhibits similar ionic radius as  $Ca^{2+}$  (Shannon, 1976). This signifies that apatite favourably comprises  $Ce^{3+}$  and  $Eu^{3+}$  instead of  $Ce^{4+}$  and  $Eu^{2+}$  (Cao et al., 2012); and  $Ca^{2+}$  in the apatite can readily be substituted via  $Eu^{3+}$ ,  $Ce^{3+}$  and  $Mn^{2+}$ , therefore, these specific elements are simply adjusted into apatite structure (Cao et al., 2012). Under the oxidizing condition,  $Ce^{3+}$ ,  $Eu^{2+}$ , and  $Mn^{2+}$  can be easily changed to  $Eu^{3+}$ ,  $Ce^{4+}$ , and  $Mn^{4+}$ . Higher oxygen fugacity conditions will generate a melt with greater  $Eu^{3+}$  however, lower  $Ce^{3+}$  quantities and significant  $Eu^{3+}$  but restricted  $Ce^{3+}$  replacement in apatite produces slightly positive to negative Ce and moderate negative to positive Eu anomalies in apatite (MacDonald et al., 2013). In contrast, low oxygen fugacity conditions will generate greater  $Ce^{3+}/Ce^{4+}$  and  $Eu^{2+}/Eu^{3+}$  ratios as well as lower  $Eu^{3+}$  concentrations ratios in a magma, resulting in positive Ce and robust negative Eu anomaly in apatite. Based on these findings, we suggest that strong negative Eu anomalies produced within apatite of Lower Yangtze and Luming are the result of overall lower  $Eu^{3+}$  concentrations and greater  $Ce^{3+}/Ce^{4+}$  and  $Eu^{2+}/Eu^{3+}$  ratios. Greater  $Eu^{2+}/Eu^{3+}$ ,  $Ce^{3+}/Ce^{4+}$  ratios, and lower  $Eu^{3+}$  concentrations can be originated under low oxygen fugacity environment, if the physical conditions especially temperature, pressure, and whole rock composition remains constant (Sha and Chappell, 1999); and the apatite crystallization under low oxygen fugacity, yields intense negative Eu anomaly (Cao et al., 2012). Therefore, we suggest that under the conditions of low oxygen fugacity, the crystallization of Lower Yangtze and Luming apatites produce strong negative Eu anomalies. Nonetheless, the variability of a single element in apatite may not be valuable entirely to delineate magmatic conditions because it can be affected through numerous dynamics at the time of magmatic crystallization. For instance, plagioclase crystallization influences the amount of europium (Eu) in magma and the Eu quantity may drop owing to plagioclase fractionation (Buick et al., 2007). Similarly, the Mn amount in magma can fluctuate during the crystallization process (Chu et al., 2009). Hence, in apatite, the multi-variance elements with opposite partitioning behaviour such as europium (Eu) and cerium (Ce) can be efficiently important to demarcate discrepancies in the redox state (Pan et al., 2016).

Pan et al. (2016) presented the apatite geochemistry from granites of the Sanjiang area, exposed in the southwestern part of China and inferred that the magma redox state could be influenced based on the negative correlation of  $\delta Ce$  and  $\delta Eu$ . In the current study, the apatite  $\delta Ce$  and  $\delta Eu$  values are also deduced with negative correlation (Fig. 12a), proposing that the variations in values of  $\delta Eu$  and  $\delta Ce$  are associated to the moderate reduced state of magma. Hence, the strong negative Eu anomaly in the apatites implies that the magmas of the Luming granites, as well as Lower Yangtze granites (BSL, XSJ, MT, HYG, HMJ), have moderately reduced state. This interpretation is

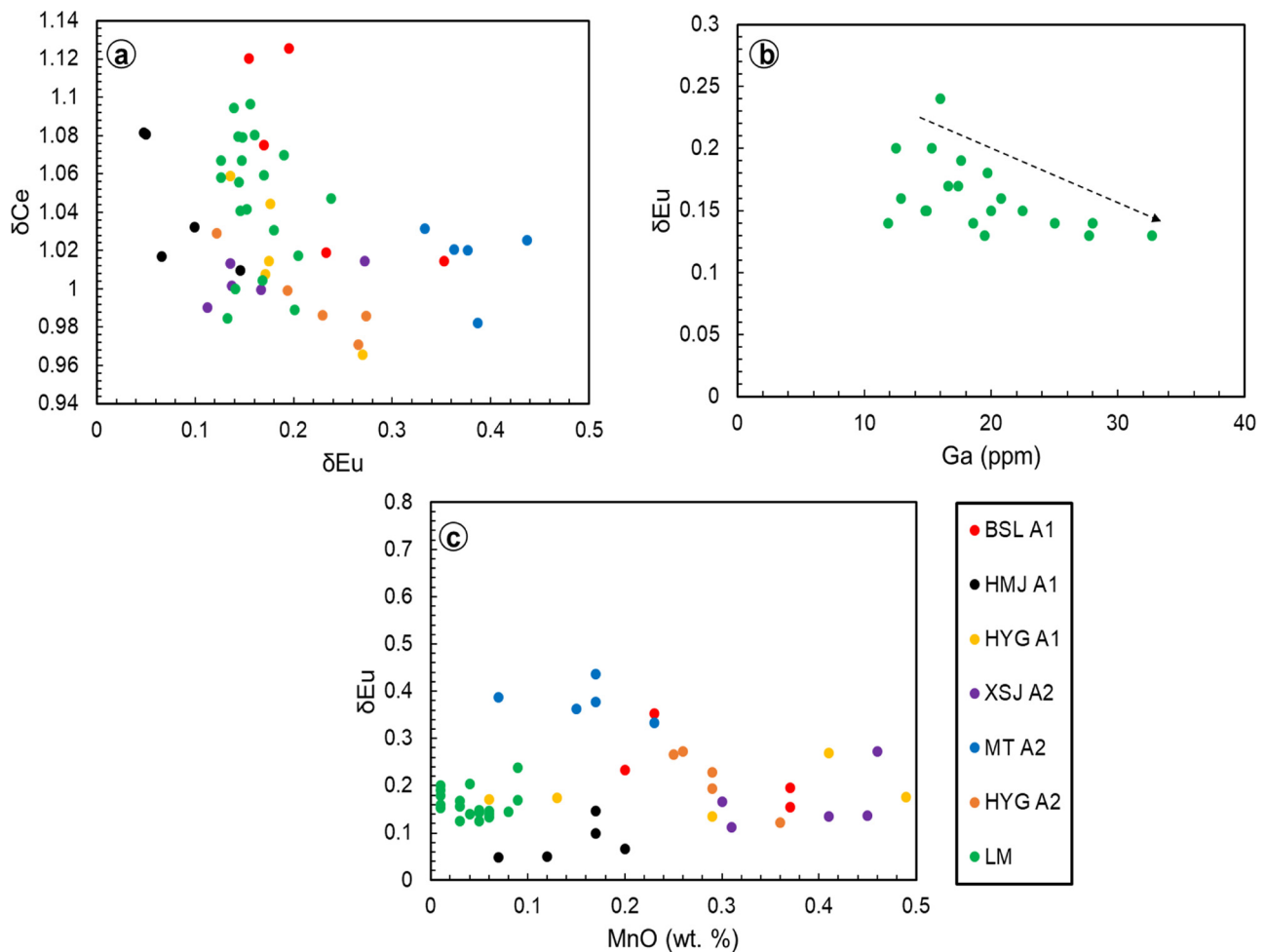


Fig. 12. Apatite plots of (a)  $\delta\text{Ce}$  vs  $\delta\text{Eu}$ . (b)  $\delta\text{Eu}$  vs Ga, and (c)  $\delta\text{Eu}$  vs MnO (wt.%) from granitic bodies of Luming and LYRB.

similar to the attributes of apatite from Mo deposits exposed in the Central Kazakhstan (Cao et al., 2012). The Ga contents (11.9–32.7 ppm, average 19.5 ppm) and  $\delta\text{Eu}$  values (0.12–0.23, average 0.16) in Luming samples are worthwhile to determine the nature of parental magma however, samples of Lower Yangtze indicate lack of Ga contents.

Ga has two states, specifically,  $\text{Ga}^{2+}$  and  $\text{Ga}^{3+}$  and  $\text{Ga}^{2+}$  is more augmented in apatite owing to its resemblance to  $\text{Ca}^{2+}$ . Therefore, if other dynamics, for instance, the Ga content of magma remain constant, a lower state of oxidation raises the Ga concentration in apatite (Pan et al., 2016). The apatite plot of  $\delta\text{Eu}$  vs Ga in the Luming granites indicates negative correlation (Fig. 12b), implying that the parental magma of the Luming granites showed moderate reduced condition.

The presence of redox-sensitive elements, for example, Eu and Mn in apatite can also be associated with the redox state of parental magma. These elements may present in diverse valence states reflecting redox states. Eu reveals two ionic valences including  $\text{Eu}^{2+}$  and  $\text{Eu}^{3+}$  (Prowatke and Klemme, 2006) whereas, Mn represents four valences namely  $\text{Mn}^{2+}$ ,  $\text{Mn}^{3+}$ ,  $\text{Mn}^{4+}$  and  $\text{Mn}^{5+}$  (Pan and Fleet, 2002). Furthermore,  $\text{Mn}^{2+}$  tends to be more augmented in apatite due to its resemblance to  $\text{Ca}^{2+}$ . The combination of  $\delta\text{Eu}$  and MnO contents are important and worthwhile to define the redox state of magma, and their negative correlation can reveal the nature of parental melts (Pan et al., 2016). In the present study, combined apatite plot of  $\delta\text{Eu}$  vs MnO in the Luming and Lower Yangtze granites express negative correlation (Fig. 12c), deducing that the parental magmas of the Luming and Lower Yangtze granites are generated under moderate reduced conditions.

#### 5.4. Apatite Sr contents and REE ratios as proxies to trace magmatic differentiation

The variation in trace elements of apatite can reveal magma compositional modification because of the crystallization of other minerals. For instance, feldspar crystallization, the leading host of Sr in silicic magma, will reduce strontium in the residual portion of melt. In this process, apatite crystallizing earlier will have greater Sr concentrations, however, apatite crystallizing late will comprise lower amounts of Sr. Therefore, the difference of Sr concentrations in apatite from rocks group can be significant to trace magmatic fractionation through this process. Rare earth element rich mineral crystallization from magma will fractionate these elements and from such magma apatite also crystallizes. Hence, the Sr concentration in apatite and ratios of REEs for instance,  $(\text{La}/\text{Yb})_N$ ,  $(\text{Sm}/\text{Yb})_N$  and  $(\text{La}/\text{Sm})_N$  are important to assess the differentiation history of granites.

As presented in Fig. 13, all of the studied apatites from granites of Lower Yangtze and Luming together confirm discrepancy and decline of  $(\text{La}/\text{Yb})_N$ ,  $(\text{La}/\text{Sm})_N$  and  $(\text{Sm}/\text{Yb})_N$  ratios with Sr concentrations. According to Pan et al., 2016, these ratios of REEs with Sr quantities indicate an important role in magma differentiation. They proposed that allanite involved in magmatic differentiation causes a decline in REEs ratios of  $(\text{La}/\text{Yb})_N$ ,  $(\text{La}/\text{Sm})_N$  and  $(\text{Sm}/\text{Yb})_N$  in apatite, however, no allanite have been observed in the Luming and Lower Yangtze samples. The Luming pluton reveals rather constant amounts of Sr in apatite. This exhibits that feldspars are not significant primary phases. Moreover, the decline in these REEs ratios with Sr concentration in Luming and most of the Lower Yangtze samples are not due to differentiation of

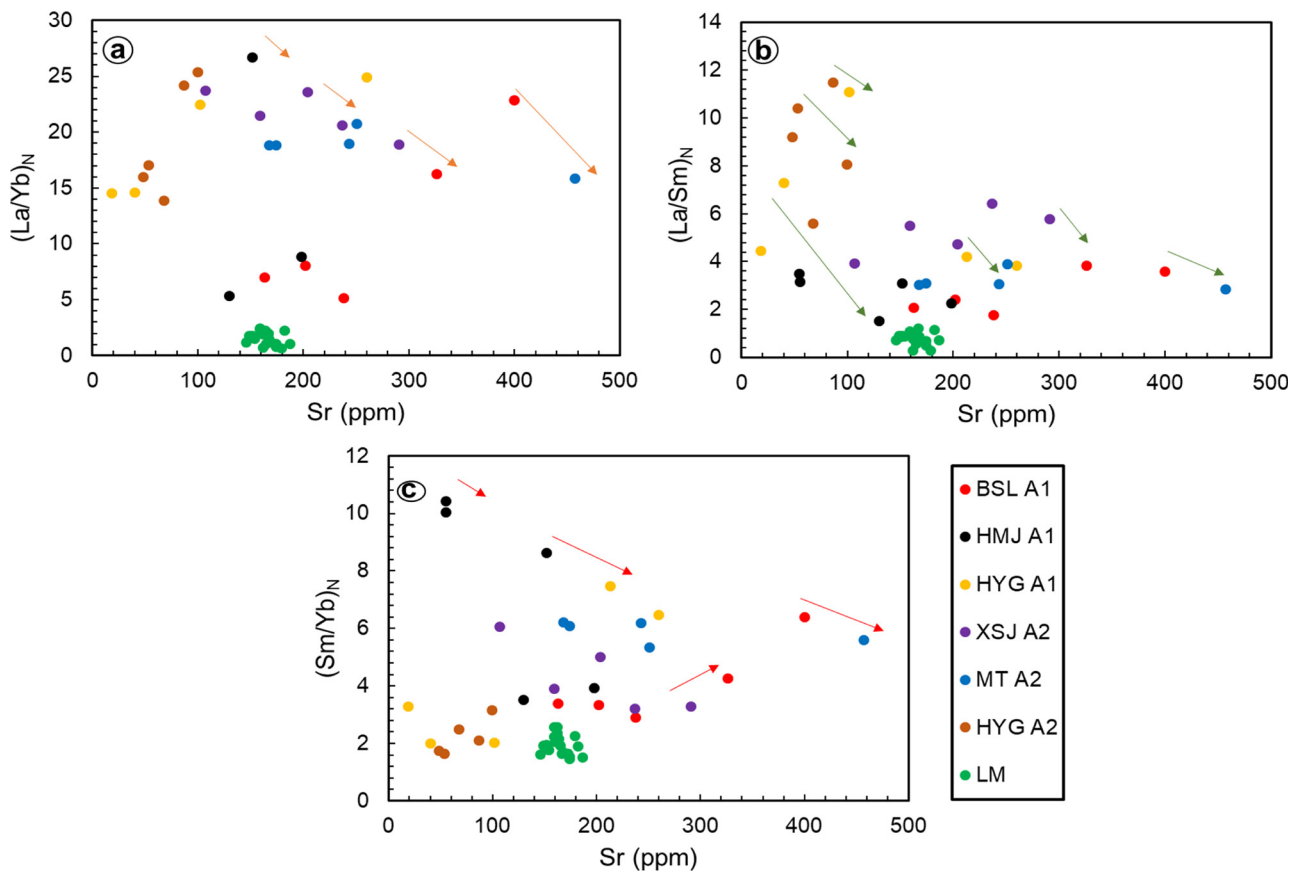


Fig. 13. Apatite plots of REEs ratios vs Sr contents for magmatic fractionation in LYRB and Luming plutons (arrows indicate variation and decline of  $(La/Yb)_N$ ,  $(La/Sm)_N$  and  $(Sm/Yb)_N$  ratios with Sr concentrations).

other light rare earth-rich minerals, since no monazite or allanite have been documented under CL images. As an alternative, the exsolution of Cl-bearing hydrotherm is a promising reason for fall in these REEs ratios. Prior researches have indicated that the exsolution of Cl-bearing hydrotherm stage might eliminate REEs from the melt (Flynn and Burnham, 1978; Keppler, 1996). Therefore, apatites formed from such melt indicate a decline in REEs ratios.

##### 5.5. Significance of apatite halogens to track magmatic volatiles and their source characteristics

Chlorine and fluorine display dynamic role during magmatic evolution by depolymerizing the melt formation and also show vigorous character in metal transport and ore deposition in case of hydrothermal process (Filiberto and Treiman, 2009; Harlov, 2015). Nonetheless, tracking the evolution of volatiles in the magmatic system is very intricate. The concentrations of Cl and F in whole-rock probably cannot immediately exhibit primary amounts of volatiles in the parental magma nevertheless, these can be assessed by minerals which are augmented in Cl and F for example, apatite (Zhang et al., 2012). Apatite has a distinctive aptitude to trace the behaviour and concentration of volatiles in the magmatic system (Webster et al., 2009). The amounts of Cl and F in the melt can be delineated from the contents of volatiles in apatite (Doherty et al., 2014). Therefore, apatite present in granitic rocks is reflected as a powerful tool to reveal the contents of magmatic volatiles and their source characteristics. In particular, apatite is a leading mineral to understand the composition of volatiles since it can concentrate volatiles directly into its crystal lattice (Harlov, 2015). All varieties of the apatites from granites of Lower Yangtze are enriched in fluorine hence, classified as fluorapatites since F is more compatible in silicate melts (Webster, 1990). Conversely, the more active Cl chemistry

shows that Cl is a more perceptible proxy comparative to F and thus can provide more geological facts. Cl is extremely compatible in apatite within a chlorine-saturated melt, even if the melt is water-saturated then chlorine is more compatible in aqueous fluids comparative to silicate melts. This indicates that amounts of chlorine do not considerably reduce during the process of fractional crystallization, representing that evolved granites can contain similar or augmented quantities of chlorine than the primary magma (Sun et al., 2007). Consequently, chlorine quantities in apatite reveal the primary Cl contents of the initial magma (Boyce et al., 2010), signifying that the amounts of volatiles of apatites from Lower Yangtze preserve the halogen compositions of actual magma.

The chlorine quantity differs in various mantle parts however, it is not considerably affected through the recycling of chlorine (Lassiter et al., 2002). Researches on submarine volcanic glasses (Stroncik and Haase, 2004) and melt inclusions resulting from mantle (Lassiter et al., 2002) propose that the mantle commonly comprises low quantities of chlorine (typically < 0.1 wt.%). This specifies that the greater amounts of chlorine in apatites from the A-type granites (BSL, XSJ, MT, HYG, HMJ) of LYRB cannot be the product of incorporation of mantle-derived material. Nevertheless, these greater amounts of chlorine are also questionable to have been resultant from melting of crustal part, principally as sedimentary material would drop more chlorine comparative to fluorine during weathering and the prior is extremely compatible in aqueous fluids, dominating to a process that accommodates fluorine in residue and reduces chlorine (Blevin and Chappell, 1992). This is the possible cause that apatite varieties in S-type granites exposed in Lachlan Fold Belt, Australia comprise predominantly < 0.1 wt.% chlorine (Sha and Chappell, 1999). Hence, the apatites of A-type granites of LYRB containing higher concentration of chlorine (0.02–1.45 wt.%, average 0.35 wt.%) must have obtained Cl from certain other fluids,

most possibly through mantle wedge melting due to fluids introduction resulting from slab convergence, a process that principally discharges brines enriched in chlorine (Lassiter et al., 2002). This fluid was most possible seawater, which amalgamated into the primitive mantle through slab convergence and discharged by dehydration of serpentine (Kawamoto et al., 2013; Reynard, 2013), implying that the Cu–Mo mineralization may be promoted in the Lower Yangtze area which can obtain an enormous amount of slab-derived fluids that also can be favourable for development of W mineralization in A-type granites. Metasomatism of the mantle wedge has been documented as an extensive process during convergence in LYRB (Jiang et al., 2018a, b) since it is linked with the consecutive release of fluids from slabs. Volatiles specifically fluorine and chlorine are contained in certain hydrous minerals and discharged during geological processes.

In A-type granites of LYRB, fluorine probably can be held by phengite and lawsonite during Paleo-Pacific Plate convergence. The lawsonite and phengite disintegration can generate fluids fertile in fluorine, responsible for mantle wedge metasomatism (Pagé et al., 2016; Schmidt and Poli, 2014). In compare, chlorine can be retained through serpentine, amphibole and chlorite, ejected prior during plate subduction (Debret et al., 2013, 2014; Deschamps et al., 2013; Pagé et al., 2016; Sun et al., 2007; Xiong et al., 2005, 2009). Chlorine can be added by the disintegration of chlorite and amphibole (Debret et al., 2014; Pagé et al., 2016; Sun et al., 2007). Likewise, chlorine can also be contributed by serpentine (Debret et al., 2013, 2014). In addition, alteration of chrysotile into antigorite may provide 90 % of chlorine (Kodolányi and Pettke, 2011) that can be considered as one more source of Cl. During slab dehydration, chlorine is extremely incompatible and favourably partitions into the liquid stage (Stronck and Haase, 2004; Sun et al., 2007), and the fluids augmented in chlorine are crucial for the transfer of metals (Keppler and Wyllie, 1991), indicating that chlorine can be important for magmas to be capable to induce Cu–Mo–W deposits.

In summary, the fluorine (1.51–3.85 wt.%, average 2.35 wt.%) and chlorine (0.02–1.45 wt.%, average 0.35 wt.%) contents of apatites in granitic rocks from Lower Yangtze deliver confirmation of slab-subduction setting and the fluids derived from slab initiated the mantle wedge melting (Ding et al., 2015), therefore, the subsequent fluids and magmas can boost the release and transportation of metals that eventually may endorse development of Cu–Mo–W mineralization in this area. On the contrary, apatites from Luming area comprises low quantities of Cl (0–0.04 wt.%, average 0.02 wt.%) and high F (3.36–5.29 wt.%, average 3.99 wt.%), suggesting that the parental magma of Luming granite is depleted in chlorine. Lower concentration of Cl and higher fluorine content in Luming apatite implies that the Luming granites are formed by partial melting of crust material and can be associated with mineralization (Blevin and Chappell, 1992). Furthermore, ratios of Cl/F of the Lower Yangtze and Luming apatite can also be pondered as crucial pointer and fingerprint to track the magmatic volatiles contents because volatiles concentrations producing from apatite composition do not fluctuate especially in crystallization interval (Zhang et al., 2012).

The apatite Cl/F ratios in Luming granites are low (0–0.01) comparative to Lower Yangtze plutons (0.007–0.96). It is generally documented that apatite is not vulnerable to subsolidus halogen exchange (Candela, 1986). Thus, this Cl/F ratio in Luming as well as Lower Yangtze apatite demonstrates the actual value in the parental magma from which they crystallized. Here we provide indirect confirmation for low Cl/F ratios in the initial magma of Luming granite since possible reasons of higher Cl contents of Lower Yangtze are discussed above. Li and Hermann (2015) presented that the low Cl concentrations in apatite represent that the host magma was deficient in chlorine. The prime reason for low chlorine content in Luming possibly can be source control. The apatite concentrations of chlorine from Luming granite are most plausibly linked to melt compositions. We propose that the parental magma of Luming pluton generated on account of partial melting

of juvenile crustal material, a source with a low Cl/F ratio. Consequently, we can suggest that slab-derived fluids containing greater Cl/F ratios (Meng, 2014); did not contribute to parental magma of Luming granite. Variations in the Cl/F values of Luming apatite have resulted from erraticism of degassing which fractionated chlorine and fluorine (Warner et al., 1998), however, these variations in Lower Yangtze apatite can be attributed to metasomatic process (Collins et al., 1982).

### 5.6. Implication for non-adakitic plutons

Based on Defant and Drummond (1990) classification, the Lower Yangtze and Luming plutons are non-adakite. However, adakitic rocks are represented by subordinate content of Y, Yb and greater Sr comparative to other kinds of silicic rocks, since adakitic magma is produced in the crust at greater depth where feldspar is unstable. While, at a shallower depth, magma comprising a higher content of Y, Yb and low concentration of Eu and Sr will be generated where feldspar indicates residual stage (Peacock et al., 1994; Rapp et al., 2002; Sen and Dunn, 1995). The Sr/Y and Eu/Eu\* ratios of apatite are important to delineate the properties of primary magma specifically the nature of parental magma. Pan et al. (2016) presented apatite chemical composition to distinguish rocks of adakitic and non-adakitic affinity in the Sanjiang area, NW China. Based on this discrimination, they suggested that the apatites which indicate adakitic character comprise higher Sr/Y and Eu/Eu\* ratios relative to other apatites that represent non-adakitic nature. These ratios of apatite can be significant to identify rocks of adakitic and non-adakitic character predominantly for those who experience hydrothermal alteration and do not sustain original Sr/Y ratios. Because apatite is not susceptible to alteration process thus can preserve real ratios of Sr/Y in comparison to feldspar which is prone to extreme alteration. Nonetheless, it would be very careful to apply this technique when apatite is not present in the primary stage. Because when apatite crystallizes due to evolving magma, it is experienced to vast fractional crystallization which probably will not indicate original ratios of Sr/Y and Eu/Eu\*. These actual ratios of parental magma will be considered when the formation of apatite is only at earlier stages (Pan et al., 2016).

The apatites in the granites of Luming indicate the occurrence of idiomorphic crystals as well as phenocrysts, whereas, apatites from Lower Yangtze granitic belts also reveal well-developed and exquisite phenocrysts (Fig. 6). These textural features of apatite imply that both of these magmatic apatites crystallized at an earlier stage hence, sustain the original ratios of Sr/Y and Eu/Eu\* which can be worthwhile to assess characteristics of parental magmas. The Sr/Y and Eu/Eu\* values of the Luming and LYRB apatites are low, plotting in the non-adakitic rock field (Fig. 14a) which suggests that the granites of Lower Yangtze and Luming are non-adakitic in nature. These interpretations and results are also consistent with the whole-rock geochemical characteristics of the Luming and LYRB granites because both are indicating non-adakitic affinities (Fig. 14b, c). Our explanations suggest that these ratios of apatite are remarkable to distinguish the adakitic character of the rock from non-adakitic ones. The non-adakitic affinity of Lower Yangtze and Luming granites is analogous with the non-adakitic characters of Cretaceous Xiuwacu in the Sanjiang region as well as Chengchao Granites exposed in the Middle Yangtze River Belt.

### 5.7. Apatite Li vs SO<sub>3</sub> and (La/Sm)<sub>N</sub> vs (Yb/Sm)<sub>N</sub> ratios as proxies for mineralization

The combination of ratios of REEs such as (La/Sm)<sub>N</sub>, (Yb/Sm)<sub>N</sub> and Li versus SO<sub>3</sub> content in apatite can be significant to define mineralization potential of a pluton. The contents and variation of S, Li, (La/Sm)<sub>N</sub>, (Yb/Sm)<sub>N</sub>, (La/Yb)<sub>N</sub> and Eu/Eu\* ratios in apatite are worthwhile to discriminate ore linked and barren granites. Those with positive correlation and broader variations can be indicative of fertile granites however, negative correlation may be suggestive of barren rocks. Our

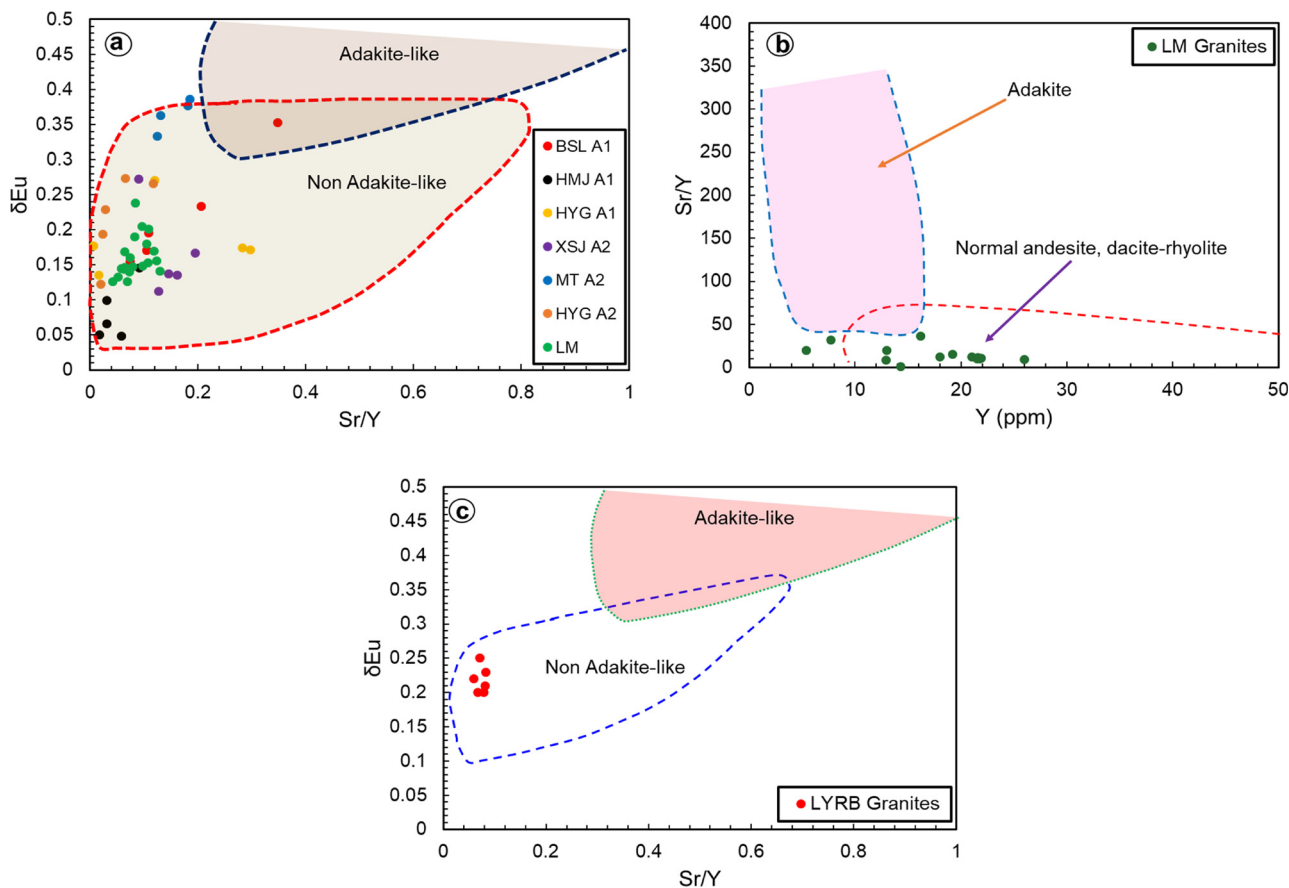


Fig. 14. (a) Plots of  $\delta\text{Eu}$  vs  $\text{Sr/Y}$  for apatites of Luming and LYRB. (b)  $\text{Sr/Y}$  vs  $\text{Y}$  for host rocks of Luming. (c)  $\delta\text{Eu}$  vs  $\text{Sr/Y}$  for host rocks of LYRB. Fields for apatites and host rocks are after Pan et al., 2016 and Drummond and Defant, 1990 respectively.

results indicate that these particular elements specifically S and Li can be more valuable to distinguish the fertile granites in a prompt and cost-effective way, and are more proficient in contrast to REEs. Li concentration is lacking in apatites of Lower Yangtze granites; however, its content in Luming apatites is in the range of 0.11–1.78 ppm in addition to  $\text{SO}_3$  (0.01–0.08 wt.%). The positive correlation of  $\text{SO}_3$  with Li in Luming apatites implies that granites of Luming are linked with ores (Fig. 15a). Moreover,  $(\text{La}/\text{Sm})_{\text{N}}$  and  $(\text{Yb}/\text{Sm})_{\text{N}}$  in apatites of Luming are in the range of (0.28–1.2) and (0.38–0.68) respectively, however, these ratios in the apatites of Lower Yangtze are (0.85–11.47) and (0.09–0.61) respectively. The combined plot of  $(\text{La}/\text{Sm})_{\text{N}}$  and  $(\text{Yb}/\text{Sm})_{\text{N}}$  in apatites of Luming and Lower Yangtze exhibit positive correlation. The positive correlation of  $(\text{La}/\text{Sm})_{\text{N}}$  and  $(\text{Yb}/\text{Sm})_{\text{N}}$  in apatites of Luming and Lower Yangtze (BSL, XSJ, MT, HYG, HMJ) suggests these rocks are ore-associated (Fig. 15b). Hence, we deduce that correlation of these REEs ratios in apatite can reveal ore potential of plutons and positive correlation between these ratios is indicative of ore-bearing rocks, however, their negative correlation is suggestive for barren rocks. The apatites  $(\text{La}/\text{Yb})_{\text{N}}$  and  $\text{Eu}/\text{Eu}^*$  ratios in ore potential granitoids may indicate fairly higher variations in contrast to barren rocks. These ratios in apatites of Luming and Lower Yangtze also reveal obvious variations, suggesting that these rocks are ore-associated (Fig. 15c). Thus, we propose that the higher variations of these apatite ratios can also be significant to discriminate ore associated as well as barren granitoids.

### 5.8. Geodynamic implications

The melting of mantle wedge material stimulated through slab-derived fluids favourably concentrates Sr linked with Th, essential to the

generation of felsic rocks particularly granitoids with the rise in  $\text{Sr}/\text{Th}$  ratios (Turner and Foden, 2001; Labanieh et al., 2012). In contrast, ratios of  $\text{La}/\text{Sm}$  are not considerably affected by partial melting; however, can be controlled by the melting of subducted oceanic sediments. The rise in melting of sediments is responsible for increment in  $\text{La}/\text{Sm}$  ratios and this melting also elevates amounts of Th, inducing stable ratios of  $\text{Sr}/\text{Th}$  (Turner and Foden, 2001; Labanieh et al., 2012). This reflects that the melting of marine sediments superimposing the subducted plate will promote ratios of  $\text{Sr}/\text{Th}$  to remain stable; however, it will elevate the  $\text{La}/\text{Sm}$  ratios in subsequent magmas. While the involvement of slab-derived fluids will equilibrate  $\text{La}/\text{Sm}$  ratios and raise the  $\text{Sr}/\text{Th}$  ratios in causing magmas. These two significant schemes can be recognized in  $\text{La}/\text{Sm}$  vs  $\text{Sr}/\text{Th}$  plot (Fig. 16). At present, there is ambiguity whether the ratios of  $\text{La}/\text{Sm}$  vs  $\text{Sr}/\text{Th}$  in mother rocks can be attained by magmatic apatite.

In felsic melts, Sr can enter into crystal lattice of apatite through replacement of Ca, while REEs and Th are commonly entered into apatite structure by other replacements, for example:  $\text{REE}^{3+} + \text{Na}^+ = 2\text{Ca}^{2+}$ ;  $\text{REE}^{3+} + \text{Si}^{4+} = \text{Ca}^{2+} + \text{P}^{5+}$ ;  $\text{Th}^{4+} + 2\text{Si}^{4+} = \text{Ca}^{2+} + 2\text{P}^{5+}$  (Sha and Chappell, 1999; MacDonald et al., 2013). These elements reveal high partition coefficients with the exemption of Th and are compatible in apatite (Prowatke and Klemme, 2006), implying that the amounts of these specific elements in apatite exhibit the quantities in host rock to a certain extent (Chu et al., 2009). The  $\text{La}/\text{Sm}$  ratios in the Luming apatites are (0.44–1.91, average 1.23). Meanwhile,  $\text{Sr}/\text{Th}$  ratios (4.29–26.82 average 15.47) of these apatites are lower, indicating no involvement of slab-derived fluids. The reliability of these values means that they will not considerably change the trends in binary plot of  $\text{Sr}/\text{Th}$  vs  $\text{La}/\text{Sm}$  (Fig. 16).

Tectonically, the Luming region was represented by the progression

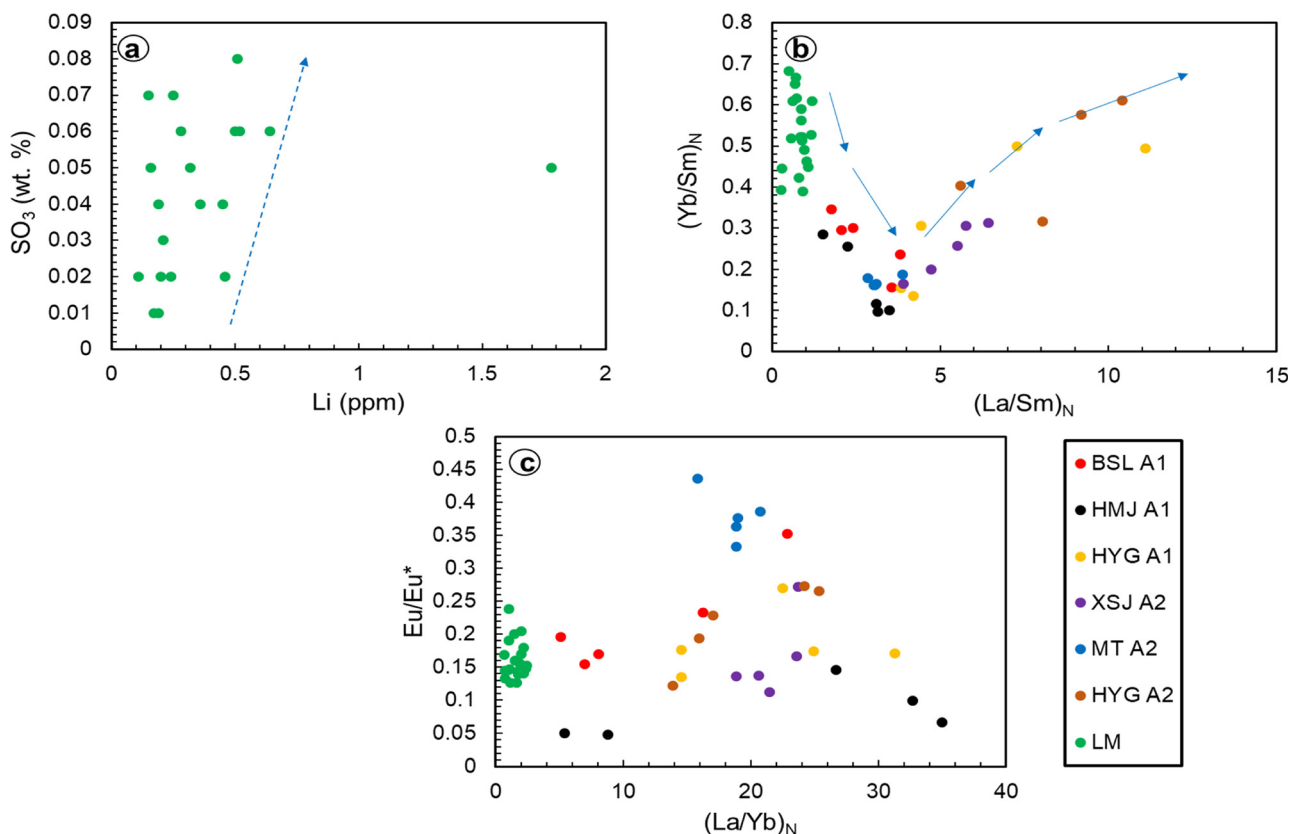


Fig. 15. Apatite binary plots for ore associated plutons of Luming (LM) and LYRB. (a) Li (ppm) vs SO<sub>3</sub> (wt.%). (b) (La/Sm)<sub>N</sub> vs (Yb/Sm)<sub>N</sub>. (c) (La/Yb)<sub>N</sub> vs Eu/Eu\*. (Arrows indicate positive correlation between (La/Sm)<sub>N</sub> vs (Yb/Sm)<sub>N</sub> and SO<sub>3</sub> with Li).

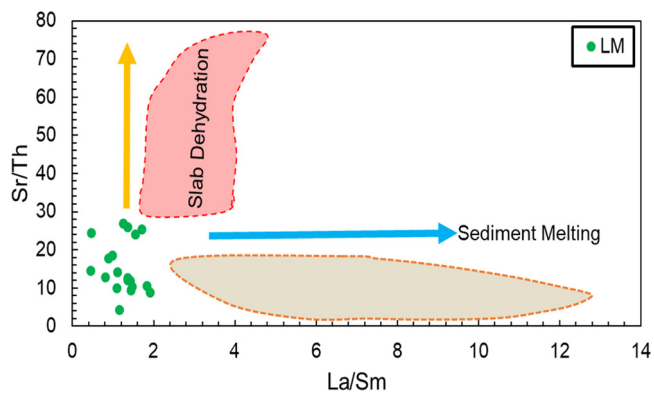


Fig. 16. Plot of Sr/Th and La/Sm ratios for apatites of Luming indicating no association with sediment melting and slab dehydration. The fields are after Ding et al. (2015).

of the Mongol-Okhotsk Ocean to the NW part and the Paleo-Pacific Ocean to the eastern part, provoking widespread magmatism during the Mesozoic (Wu et al., 2011). The convergence of the Paleo-Pacific Plate is probably responsible for early Jurassic magmatism and metallogenic specificity in the Luming area. In general, giant porphyry Mo granitic deposits developed in this area in Mesozoic, making Luming a dynamic and renowned Mo bearing place in China and worldwide (Chen et al., 2017; Qin et al., 2017). According to Hu et al., 2014, the magmas of Luming granites were produced as a result of the partial melting of depleted lithospheric mantle and metasomatized through subducted fluids released from the slab. In contradiction with Hu et al., 2014, based on the apatite plot of Sr/Th and La/Sm, the Mo bearing granites of Luming provide no evidence of any association with slab-derived material or sediment melting (Fig. 16). The apatite geochemistry from

Luming exhibits that the parental magma of these granites are Cl deficient (0–0.04 wt.%, average 0.02 wt.%), fairly high F (3.36–5.29 wt.%, average 3.99 wt.%), high F/Cl ratios (89.5–245), La/Sm (0.44–1.91, average 1.23) and lower Sr/Th ratios (4.29–26.82 average 15.47), suggesting strong clues that these granites are developed from magmas, produced as a result of partial melting of juvenile crustal material. Our finding is consistent with Chen and Zhang, 2018 who proposed that based on Nd isotope characteristics, melting of juvenile crustal material is responsible for the generation of the Luming Mo–W granites.

Another explanation for this evidence is that the apatites within slab-derived granites normally reveal greater δEu and lower δCe values in comparison to apatites of other granites (derived from juvenile crustal material); (Sha and Chappell, 1999; Chu et al., 2009). Apatites of the Luming granites linked with Mo–W deposits represent low δEu (0.12–0.23; average 0.16) and high δCe (0.98–1.09; average 1.04) values (Fig. 12a), representing no association with slab dehydration. These values provide solid confirmations that these granites are originated in consequence of the partial melting of juvenile crustal material (Zhu et al., 2009).

In contrast, A-type granites of Lower Yangtze (BSL, XSJ, MT, HYG, HMJ) are associated with slab dehydration, and these granites were emplaced during the same period of 125 Ma. The heterogeneity in source constituents prompted through the subduction of the Palaeo-Pacific plate beneath Southeast China, indicated a dynamic role in the development of coexisting A<sub>1</sub> and A<sub>2</sub>-type granites (Jiang et al., 2018b). Previous researches explored that these granites are associated with uranium and gold mineralization, however, in the present study, apatite geochemistry suggests that these granites are also linked with Cu–Mo–W mineralization (Fig. 17 and 19).

Here, we relate data of Cu–Mo deposits of Lower Yangtze Belt to apatites from Cu–Mo deposits of the Central Asian Orogenic Belt (CAOB); (Cao et al., 2012). Apatites in both areas have parallel

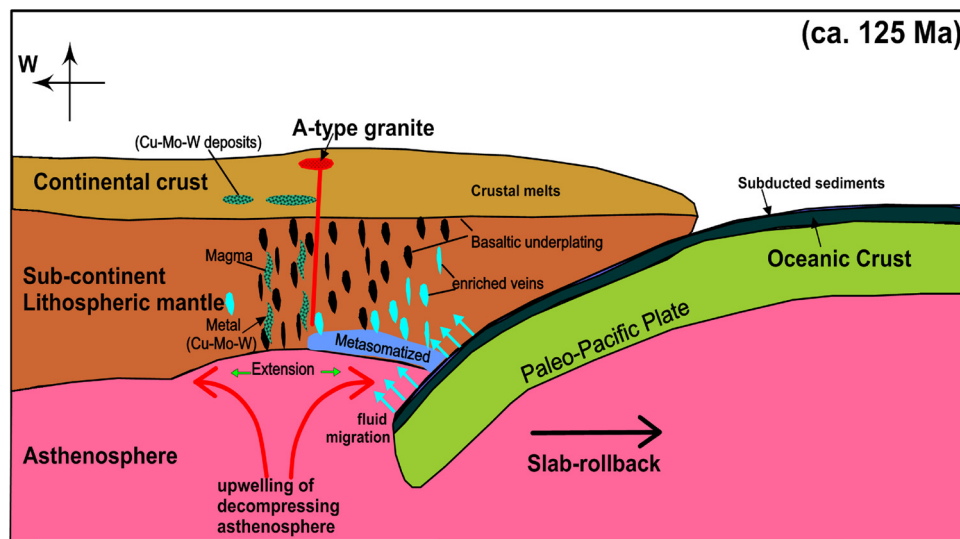


Fig. 17. Cartoon indicating tectonic evolution of A-type granites and mineralization in the LYRB.

compositions in terms of halogens (F, Cl) and Eu anomalies (Cao et al., 2012). The apatites of the CAOB express slab dehydration phenomena which is comparable to that of apatites from LYRB, suggesting that both of these deposits developed in parallel styles. On the contrary, apatites from W deposits of CAOB also deliver confirmation of sediments melting, a characteristic that is absent in apatites from Lower Yangtze Belt, signifying that the prior incorporated surplus melts resulting from marine sediments (Heinhorst et al., 2000). These marine sediments are not present in LYRB since this region was influenced by roll-back of the Paleo-Pacific Plate during the late Mesozoic era, creating an intraplate extensional setting that was free of these marine sediments. In addition, the creation of this intraplate extensional environment was prompted by lithospheric thinning and uplifting of the asthenospheric mantle during the late Mesozoic era, which assisted to yield the Cu–Mo–W mineralization in this area.

In summary, we suggest that the crustal thinning, upwelling of asthenospheric mantle and associated Cu–Mo–W mineralization in LYRB induced from the mutual impacts of the Paleo-Pacific plate subduction and intraplate extension (Fig. 17). The mineralization potential and tectonic settings of A-type granites of Lower Yangtze River Belt are comparable to Jurassic Cu–Mo–W bearing A-type granites exposed in the central Nanling region, South China.

The LYRB indicates a natural laboratory for exploration into tectonism and the generation of Cu–Mo and W deposits in this region. Linking the apatite geochemistry deliberated here with formerly attained geochemical data implies that the convergence of Paleo-Pacific Plate, triggered partial melting of mantle wedge by means of introduction of fluids released from the slab. Based on geochemical signatures of apatite enrichment of Cl (0.02–1.45 wt.%, average 0.35 wt. %), less F (1.51–3.85 wt.%, average 2.35 wt.%) as well as F/Cl ratio (1.04–131.5, average 46.14) and stable La/Sm ratios (2.42–18.24, average 7.84), in contrast to Luming suggests that the magmas of these rocks are associated with slab dehydration.

Apart from these aspects, magmas of A-type granites are commonly being linked with slab dehydration whereas, magmas of S-type granites are related with crustal partial melting (Ishihara, 1981; Blevin and Chappell, 1992, 1995; Bryant et al., 2007). Apatites within A-type granites normally reveal greater  $\delta\text{Eu}$  and lower  $\delta\text{Ce}$  values in comparison to apatites of S-type granites (Sha and Chappell, 1999; Chu et al., 2009). Apatites within the Yangtze A-type granitic rocks associated with Cu–Mo–W mineralization indicate higher  $\delta\text{Eu}$  values (0.04–0.43; average 0.21) and lower  $\delta\text{Ce}$  values (0.96–1.12; average 1.02; Fig. 12a), proposing another strong clue that these granites have an association with slab dehydration.

In light of these findings, we suggest that the apatite chemistry is a valuable and powerful proxy to evaluate the geodynamic evolution of granites.

#### 5.9. Apatite as vigorous tool to pinpoint polymetallic mineralization and fingerprint for ore varieties

As indicated above that the chemistry of apatite mainly its trace elements and halogen composition typically represent magmatic conditions. This, together with the fact that apatite is less vulnerable to the process of hydrothermal alteration, is measured as the main aspect of fertile granites and making apatite as an important and dynamic tool for evaluating the mineralization perspective of Lower Yangtze and Luming granites. Moreover, its geochemical depiction can be vital to assess the degree of magmatic fractionation. For instance, Fig. 18 shows obvious variation and positive correlation between F/Cl ratios and F contents which is representation of magmatic differentiation supported through silica content of whole rock of Luming and Yangtze ranging from 67.78 to 82.14 wt.%; and 64–76.6 wt.% respectively (the calculated data for whole rock  $\text{SiO}_2$  content in Yangtze granites are from Yang et al., 2017; Jiang et al., 2018b whereas, Luming granites  $\text{SiO}_2$  values are from Hu et al., 2014 and Liu et al., 2014). This clarification about magmatic fractionation is comparable to the findings of (Cao et al., 2012). In addition, the rise in fluorine content in fluorapatites of the Yangtze as well as Luming is mainly due to fractionation (Nash, 1984). Similarly, the negative correlation of Sr vs Y and  $(\text{La}/\text{Yb})_N$  vs Sr

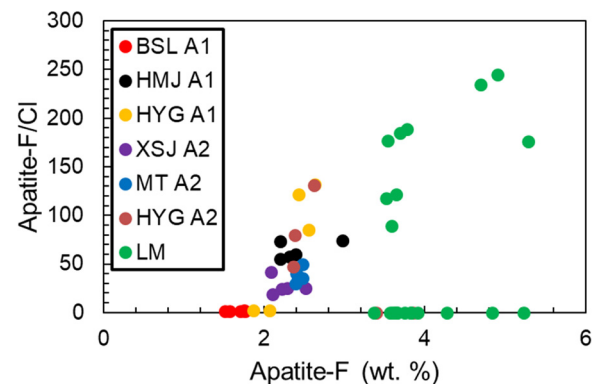


Fig. 18. Plot of F/Cl ratio vs F (wt.%) for apatites of Luming (LM) and Lower Yangtze Belt (BSL, XSJ, MT, HYG, HMJ).

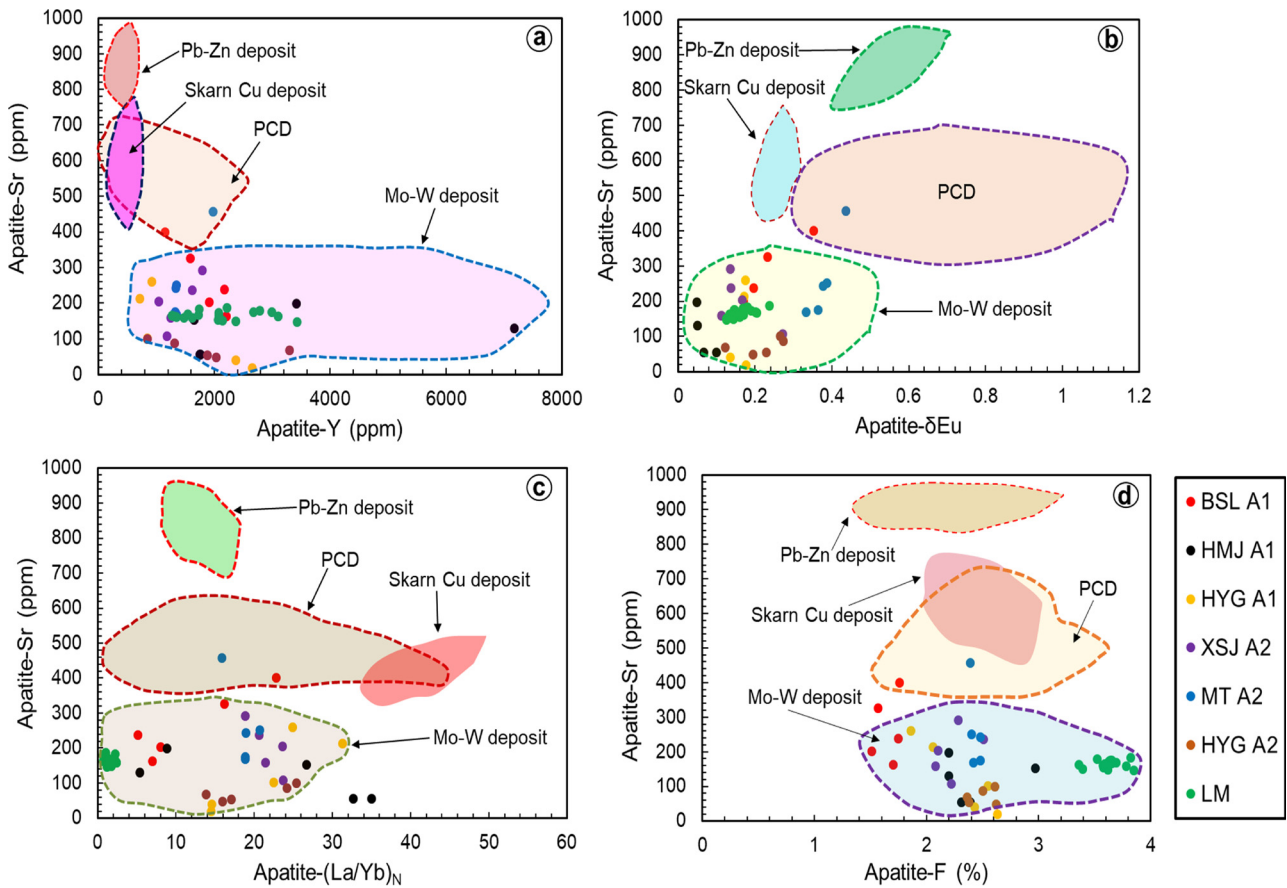


Fig. 19. Apatite discrimination plots from granites of Luming (LM) and LYRB. (a) Y (ppm) vs Sr (ppm). (b) δEu vs Sr (ppm). (c) (La/Yb)<sub>N</sub> vs Sr (ppm). (d) F (wt.%) vs Sr (ppm). The fields are after Cao et al. (2012).

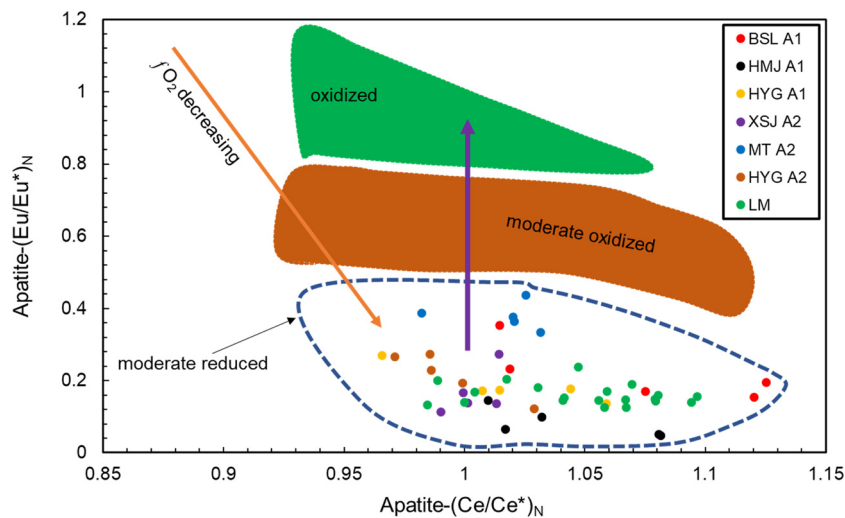


Fig. 20. Apatite plot of (Eu/Eu\*)<sub>N</sub> and (Ce/Ce\*)<sub>N</sub> from granites of Luming (LM) and Lower Yangtze Belt (BSL, XSJ, MT, HYG, HMJ). The fields are after Cao et al. (2012).

in apatite displays differentiation (Fig. 19 a, c). Various natures of ore deposits are linked to distinct differentiated magma of Lower Yangtze and Luming together with moderately reduced state of magma, hence different categories of deposits show diverse characters of Sr, δEu, Y and (La/Yb)<sub>N</sub> in apatite (Fig. 19).

The magmatic apatites of Lower Yangtze and Luming have several geochemical features, important to discriminate their associated mineral deposits. Through apatite geochemistry and portrayal of binary plots, we recognized two forms of ore deposits in Lower Yangtze and

single economic deposit in the Luming area. Apatite plot of Y (ppm) and Sr (ppm) shows that Mo-W deposits of Lower Yangtze (BSL, XSJ, MT, HYG, HMJ) are characterized by slightly higher Y and greater Sr in comparison to Luming. Further, certain samples from Lower Yangtze granites (BSL, MT) also suggest occurrence of Cu mineralization with higher content of Sr. Apatite plot of Sr vs δEu and (La/Yb)<sub>N</sub> vs Sr (ppm) exhibits that Mo-W and Cu deposits of Lower Yangtze are distinguished by higher Sr, δEu and (La/Yb)<sub>N</sub> in contrast to Luming Mo-W deposits. The F% and Sr (ppm) plotting displays that Mo-W and Cu deposits of

Lower Yangtze are represented by higher Sr and lower F content in comparison to Luming Mo–W deposits. Hence, based on these interpretations, we can propose that the contents of Sr,  $\delta\text{Eu}$ , Y, F and  $(\text{La}/\text{Yb})_N$  in apatite can be worthwhile to prove the degree of fractionation and pinpoint varieties of ore deposits (Figs. 18 and 19).

Granitic rocks linked with Cu mineralization commonly form from oxidized nature of magmas, however, can be produced from moderate reduced magma (Cao et al., 2012). The granites associated with Mo–W mineralization can be generated from either oxidized or reduced felsic magmas (Meinert et al., 2005; Cao et al., 2012; Sun et al., 2013). In the present study, the geochemistry of apatites indicates that the granitic rocks of Lower Yangtze are associated with Cu–Mo–W however, granites of Luming are linked with Mo–W mineralization (Fig. 19). Based on strong negative europium anomaly and plot of  $(\text{Ce}/\text{Ce}^*)_N$  and  $(\text{Eu}/\text{Eu}^*)_N$  (Fig. 20), we suggest that the mineralization and ore varieties in granites of Lower Yangtze and Luming developed in moderated reduced states of magma under lower oxygen fugacity which is consistent with the findings of (Cao et al., 2012). Our interpretation contradicts the observation of Jiang et al., 2018a who proposed that A-type granites of Lower Yangtze are developed under oxidized as well as reduced states of magma.

### 5.10. Implications for exploration of Cu–Mo–W deposits

Prior geological researches in the LYRB revealed that A-type granites are associated principally with uranium and gold mineralization, however, except this mineralization, the present study first time explores Cu–Mo–W deposits in this belt and propose a new tectonic model of the deposits based upon apatite geochemistry which is comparable to widely exposed Jurassic A-type granites of Central Nanling region in term of mineralization and tectonic settings. Previous geological investigations focused on geochemistry and regional metallogenic features in the Luming granitic rocks and revealed that these granites are Mo bearing (Chen et al., 2017). In this study, based on apatite geochemistry, we further confirm that these rocks contain Mo–W deposits and exhibit similar characteristics of Jurassic Mo deposits of Luming. This research work confirms that Sr,  $\delta\text{Eu}$ , Y, F and  $(\text{La}/\text{Yb})_N$ , Li versus  $\text{SO}_3$  and  $(\text{La}/\text{Sm})_N$  ratio versus  $(\text{Yb}/\text{Sm})_N$  in apatite are important to distinguish ore-bearing and barren granitic rocks in the Luming as well as Lower Yangtze Belt. This, together with the characteristic that apatite is less vulnerable to alteration process, can be reflected as primary feature of mineralized granites. Therefore, these might be broad-spectrum attributes of mineralized plutons in the Yangtze Belt as well as the Luming area, however, it still awaits confirmation from data on other deposits of Yangtze and Luming, which are present in same geological settings. Additionally, our study displays  $(\text{Eu}/\text{Eu}^*)_N$  ratios (0.20), higher Cl contents and greater Cl/F ratios of Yangtze apatite, which can be reflected as characteristics of mineralized rock. Although the rocks of Luming are represented by low chlorine content, these are mineralized indicating that volatiles are not considered as powerful proxies to discriminate mineralized and unmineralized plutons. If these outcomes are confirmed by further research works, then the evaluation of concentrations of apatite will deliver a valuable tool not only in differentiating fertile and barren rocks at an early phase of exploration but also in assessing the prospective mineralization varieties for particular plutons.

## 6. Concluding remarks

Most significant findings from this research can be summarized in the following orders:

- (1) The apatites of Luming and Lower Yangtze can be characterized as fluorapatites and based on their textural features, fluorapatites characteristic and  $\text{SiO}_2$ -MnO plot; we can advocate that these are magmatic apatites, free from perceptible alteration and significant

to reflect the actual attributes of parental melts.

- (2) The apatites indicate strong negative Eu anomalies that are inducing from plagioclase crystallization earlier than apatite. The noticed concentrations of major and trace elements in both apatites were predominantly controlled by their contents in parental melts and partitioning between apatite/melt or competing minerals. Moreover, the combined plot of  $\Sigma\text{REE}$  with host rocks  $\text{SiO}_2$  contents suggests that the  $\Sigma\text{REE}$  amounts in apatites are principally governed by  $\text{SiO}_2$  in the melt.
- (3) The trace elements in apatites of Lower Yangtze and Luming are controlled by titanite crystallization and crystal fractionation of apatite respectively. Exsolution of Cl-bearing fluid is the main cause of lower  $(\text{La}/\text{Sm})_N$  values in Luming apatite while the higher  $(\text{La}/\text{Sm})_N$  values in Lower Yangtze apatites are due to titanite governance. We suggest that the incorporation of more mafic magma and restricted feldspar crystallization in Lower Yangtze apatite in contrast to Luming are promising cause of higher contents of Sr.
- (4) The negative correlation of  $\delta\text{Eu}$  vs Mn,  $\delta\text{Eu}$  vs  $\delta\text{Ce}$  and  $\delta\text{Eu}$  vs Ga, as well as the presence of strong negative Eu anomalies, advocate that the parental magmas of the Luming and Lower Yangtze granites are generated under moderately reduced conditions.
- (5) Apatite Sr contents and REE ratios particularly  $(\text{La}/\text{Yb})_N$ ,  $(\text{Sm}/\text{Yb})_N$  and  $(\text{La}/\text{Sm})_N$  are documented as significant proxies to trace the differentiation history of both granites.
- (6) Contents of apatite volatiles can reveal the halogens augmentation or paucity in the host rocks, those apatites comprising more chlorine and less fluorine are linked with slab dehydration while apatites with lower Cl and higher F contents implies association with partial melting of lower crust material.
- (7) The apatites composition suggests that both granites are non-adakitic in nature, consistent with the host rocks non-adakitic affinities.
- (8) The contents of  $\text{SO}_3$  and Li in apatites can be more valuable to distinguish the fertile granites in a prompt and cost-effective way and are more proficient in contrast to REEs. The positive correlation of  $\text{SO}_3$  with Li,  $(\text{La}/\text{Sm})_N$  vs  $(\text{Yb}/\text{Sm})_N$  and obvious variations of  $(\text{La}/\text{Yb})_N$  vs  $\text{Eu}/\text{Eu}^*$  implies that the host rocks are ore-associated.
- (9) High F/Cl ratios, stable La/Sm ratios, highest  $\delta\text{Eu}$  and lowest  $\delta\text{Ce}$  values in Lower Yangtze apatites suggest solid clues that the magmas of these granites have association with slab dehydration. Based on apatite geochemistry, we propose that the crustal thinning, upwelling of asthenospheric mantle and associated Cu–Mo–W mineralization in Lower Yangtze is induced from the mutual impacts of Paleo-Pacific plate subduction and intraplate extension. However, fairly high F/Cl ratios, stable La/Sm, lowest  $\delta\text{Eu}$ , highest  $\delta\text{Ce}$ , and Sr/Th ratios of Luming apatites imply that Mo–W bearing granites are originated in consequence of partial melting of juvenile crustal material.
- (10) Apatite contents of Sr,  $\delta\text{Eu}$ , Y, F and  $(\text{La}/\text{Yb})_N$  are worthwhile to pinpoint polymetallic mineralization and fingerprint for ore varieties. Strong negative Eu anomalies and plot of  $(\text{Ce}/\text{Ce}^*)_N$  and  $(\text{Eu}/\text{Eu}^*)_N$  suggest that the Cu–Mo–W mineralization developed in moderate reduced states of magma under low oxygen fugacity.

## Declaration of Competing Interest

The authors declare that they have no known competing financial interests or personal relationships that could have appeared to influence the work reported in this paper.

## Acknowledgments

This project was funded by the Chinese Academy of Sciences and

Chinese NSF Projects (41673051, 41872097), the ARC Centre of Excellence-linking fund (P2A3). Mr. Tehseen is extremely thankful to the Chinese Academy of Sciences for sponsoring this research project. We wish to express our appreciation to Xing-Chun Zhang and Wei Terry Chen for their fruitful discussion. The constructive reviews of Professor Irina Artemieva (Editor-in-Chief) and anonymous reviewers have significantly improved the quality of the manuscript.

## Appendix A. Supplementary data

Supplementary material related to this article can be found, in the online version, at doi:<https://doi.org/10.1016/j.jog.2020.101723>.

## References

- Aigner-Torres, M., Blundy, J., Ulmer, P., Pettko, T., 2007. Laser ablation ICPMS study of trace element partitioning between plagioclase and basaltic melts: an experimental approach. *Contrib. Mineral. Petrol.* 153, 647–667.
- Azadabakht, Z., Lentz, D., McFarlane, C., 2018. Apatite chemical compositions from acadian-related granitoids of New Brunswick, Canada: implications for petrogenesis and metallogenesis. *Minerals* 8, 598.
- Bea, F., 1996. Residence of REE, Y, Th and U in granites and crustal protoliths; implications for the chemistry of crustal melts. *J. Petrol.* 37, 521–552.
- Belousova, E.A., Walters, S., Griffin, W.L., O'Reilly, S.Y., 2001. Trace-element signatures of apatites in granitoids from the Mt Isa Inlier, northwestern Queensland. *Austrian J. Earth Sci.* 48, 603–619.
- Belousova, E.A., Griffin, W.L., O'Reilly, S.Y., Fisher, N.I., 2002. Apatite as an indicator mineral for mineral exploration: trace-element compositions and their relationship to host rock type. *J. Geochem. Explor.* 76, 45–69.
- Blevin, P.L., Chappell, B.W., 1992. The role of magma sources, oxidation states and fractionation in determining the granite metallogeny of eastern Australia. *Earth and Environ. Sci. Trans. Roy. Soc. Edinb.* 83, 305–316.
- Blevin, P.L., Chappell, B.W., 1995. Chemistry, origin, and evolution of mineralized granites in the Lachlan fold belt, Australia; the metallogeny of I- and S-type granites. *Econ. Geol.* 90, 1604–1619.
- Boyce, J.W., Liu, Y., Rossman, G.R., Guan, Y., Eiler, J.M., Stolper, E.M., Taylor, L.A., 2010. Lunar apatite with terrestrial volatile abundances. *Nature* 466, 466–470.
- Bryant, J.A., Yagodinski, G.M., Churikova, T.G., 2007. Melt-mantle interactions beneath the Kamchatka arc: Evidence from ultramafic xenoliths from Shiveluch volcano. *Geochim. Geophys. Res.* <https://doi.org/10.1029/2006GC001443>.
- Buick, I.S., Hermann, J., Maas, R., Gibson, R.L., 2007. The timing of sub-solidus hydrothermal alteration in the Central Zone, Limpopo Belt (South Africa): constraints from titanite U–Pb geochronology and REE partitioning. *Lithos* 98, 97–117.
- Candela, P.A., 1986. Toward a thermodynamic model for the halogens in magmatic systems: an application to melt-vapor-apatite equilibria. *Chem. Geol.* 57, 289–301.
- Cao, M., Li, G., Qin, K., Seitmuratova, E.Y., Liu, Y., 2012. Major and trace element characteristics of apatites in granitoids from Central Kazakhstan: implications for petrogenesis and mineralization. *Resour. Geol.* 62, 63–83.
- Chen, W., Simonetti, A., 2014. Evidence for the multi-stage petrogenetic history of the Oka carbonatite complex (Québec, Canada) as recorded by perovskite and apatite. *Minerals* 4, 437–476.
- Chen, Y.J., Zhang, C., Li, N., Yang, Y.F., Deng, K., 2012. Geology of the Mo deposits in Northeast China. *J. Jilin Univ.* (Earth Science Edition) 42, 1223–1268.
- Chen, Y.J., Zhang, C., Wang, P., Pirajno, F., Li, N., 2017. The Mo deposits of Northeast China: a powerful indicator of tectonic settings and associated evolutionary trends. *Ore Geol. Rev.* 81, 602–640.
- Chen, L., Zhang, Y., 2018. In situ major, trace-elements and Sr–Nd isotopic compositions of apatite from the Luming porphyry Mo deposit, NE China: constraints on the petrogenetic-metallogenetic features. *Ore Geol. Rev.* 94, 93–103.
- Chew, D.M., Donelick, R.A., 2012. Combined apatite fission track and U–Pb dating by LA-ICP-MS and its application in apatite provenance analysis. *Quantitative Mineralogy and Microanalysis of Sediments and Sedimentary Rocks Volume 42*. Mineralogical Association of Canada, Short Course, pp. 219–247.
- Chu, M.F., Wang, K.L., Griffin, W.L., Chung, S.L., O'Reilly, S.Y., Pearson, N.J., Izuka, Y., 2009. Apatite composition: tracing petrogenetic processes in Trans Himalayan granitoids. *J. Petrol.* 50, 1829–1855.
- Collins, W.J., Beams, S.D., White, A.J.R., Chappell, B.W., 1982. Nature and origin of A-type granites with particular reference to southeastern Australia. *Contrib. Mineral. Petrol.* 80, 189–200.
- Creaser, R.A., Gray, C.M., 1992. Preserved initial  $^{87}\text{Sr}/^{86}\text{Sr}$  in apatite from altered felsic igneous rocks: a case study from the Middle Proterozoic of South Australia. *Geochim. Cosmochim. Acta* 56, 2789–2795.
- Debert, B., Nicollet, C., Andreani, M., Schwartz, S., Godard, M., 2013. Three steps of serpentinization in an eclogitized oceanic serpentization front (Lanzo Massif–Western Alps). *J. Metamorph. Geol.* 31, 165–186.
- Debert, B., Koga, K.T., Nicollet, C., Andreani, M., Schwartz, S., 2014. F, Cl and S input via serpentinization in subduction zones: implications for the nature of the fluid released at depth. *Terra Nova* 26, 96–101.
- Defant, M.J., Drummond, M.S., 1990. Derivation of some modern arc magmas by melting of young subducted lithosphere. *Nature* 347, 662–665.
- Deschamps, F., Godard, M., Guillot, S., Hattori, K., 2013. Geochemistry of subduction zone serpentinites: a review. *Lithos* 178, 96–127.
- Ding, T., Ma, D., Lu, J., Zhang, R., 2015. Apatite in granitoids related to polymetallic mineral deposits in southeastern Hunan Province, Shi–hang zone, China: implications for petrogenesis and metallogenesis. *Ore Geol. Rev.* 69, 104–117. <https://doi.org/10.1016/j.oregeorev.2015.02.004>.
- Doherty, A.L., Webster, J.D., Goldoff, B.A., Piccoli, P.M., 2014. Partitioning behavior of chlorine and fluorine in felsic melt–fluid (s)–apatite systems at 50 MPa and 850–950°C. *Chem. Geol.* 384, 94–111.
- Drake, M.J., 1975. The oxidation state of europium as an indicator of oxygen fugacity. *Geochim. Cosmochim. Acta* 39, 55–64.
- Filiberto, J., Treiman, A.H., 2009. The effect of chlorine on the liquidus of basalt: first results and implications for basalt genesis on Mars and Earth. *Chem. Geol.* 263, 60–68.
- Flynn, R.T., Burnham, C.W., 1978. An experimental determination of rare earth partition coefficients between a chloride containing vapor phase and silicate melts. *Geochim. Cosmochim. Acta* 42, 685–701.
- Fujimaki, H., 1986. Partition coefficients of Hf, Zr, and REE between zircon, apatite, and liquid. *Contrib. Mineral. Petrol.* 94, 42–45.
- Ge, W., Wu, F., Zhou, C., Rahman, A.A., 2005. Emplacement age of the Tahe granite and its constraints on the tectonic nature of the Ergun block in the northern part of the Da Hinggan Range. *Chin. Sci. Bull.* 50, 2097–2105.
- Glorie, S., De Grave, J., Buslov, M.M., Zhimulev, F.I., Izmer, A., Vandoorne, W., Ryabinin, A., Vanhaecke, F., Elburg, M.A., 2011. Formation and Palaeozoic evolution of the Gorny–Altai–altai–Mongolia suture zone (South Siberia): zircon U/Pb constraints on the igneous record. *Gondwana Res.* 20, 465–484.
- Harlov, D.E., 2015. Apatite: a fingerprint for metasomatic processes. *Elements* 11, 171–176.
- Heinhorst, J., Lehmann, B., Ermolov, P., Serykh, V., Zhurutin, S., 2000. Paleozoic crustal growth and metallogeny of Central Asia: evidence from magmatic-hydrothermal ore systems of Central Kazakhstan. *Tectonophysics* 328, 69–87.
- Henrichs, I.A., O'Sullivan, G., Chew, D.M., Mark, C., Babechuk, M.G., McKenna, C., Emo, R., 2018. The trace element and U–Pb systematics of metamorphic apatite. *Chem. Geol.* 483, 218–238.
- Hoskin, P.W., Kinny, P.D., Wyborn, D., Chappell, B.W., 2000. Identifying accessory mineral saturation during differentiation in granitoid magmas: an integrated approach. *J. Petrol.* 41, 1365–1396.
- Hu, X., Ding, Z., He, M., Yao, S., Zhu, B., Shen, J., Chen, B., 2014. A porphyry-skarn metallogenetic system in the lesser Xing'an range, NE China: implications from U–Pb and Re–Os geochronology and Sr–Nd–Hf isotopes of the Luming Mo and xulaojiugou Pb–Zn deposits. *J. Asian Earth Sci.* 90, 88–100.
- Ishihara, S., 1981. The granitoid series and mineralization. *Econ. Geol.* 458–484.
- Jahn, B.M., Litvinovsky, B.A., Zanzivich, A.N., Reichow, M., 2009. Peralkaline granitoid magmatism in the Mongolian–transbaikalian Belt: evolution, petrogenesis and tectonic significance. *Lithos* 113, 521–539.
- Jiang, X.Y., Li, H., Ding, X., Wu, K., Guo, J., Liu, J.Q., Sun, W.D., 2018a. Formation of A-type granites in the Lower Yangtze River Belt: a perspective from apatite geochemistry. *Lithos* 304, 125–134.
- Jiang, X.Y., Ling, M.X., Wu, K., Zhang, Z.K., Sun, W.D., Sui, Q.L., Xia, X.P., 2018b. Insights into the origin of coexisting A1- and A2-type granites: implications from zircon Hf–O isotopes of the Huayuangong intrusion in the Lower Yangtze River Belt, eastern China. *Lithos* 318, 230–243.
- Kawamoto, T., Yoshikawa, M., Kumagai, Y., Mirabueno, M.H.T., Okuno, M., Kobayashi, T., 2013. Mantle wedge infiltrated with saline fluids from dehydration and decarbonation of subducting slab. *Proc. Natl. Acad. Sci.* 110, 9663–9668.
- Keppeler, H., 1996. Constraints from partitioning experiments on the composition of subduction-zone fluids. *Nature* 380, 237–240.
- Keppeler, H., Wyllie, P.J., 1991. Partitioning of Cu, Sn, Mo, W, U, and Th between melt and aqueous fluid in the systems haplogranite–H<sub>2</sub>O–HCl and haplogranite–H<sub>2</sub>O–HF. *Contrib. Mineral. Petrol.* 109, 139–150.
- Kodolányi, J., Pettko, T., 2011. Loss of trace elements from serpentinites during fluid-assisted transformation of chrysotile to antigorite—an example from Guatemala. *Chem. Geol.* 284, 351–362.
- Krneta, S., Ciobanu, C.L., Cook, N.J., Ehrig, K., Kontonikas-Charos, A., 2016. Apatite at Olympic Dam, South Australia: a petrogenetic tool. *Lithos* 262, 470–485.
- Labanieh, S., Chauvel, C., Germa, A., Quidelleur, X., 2012. Martinique: a clear case for sediment melting and slab dehydration as a function of distance to the trench. *J. Petrol.* 53, 2441–2464.
- Lassiter, J.C., Hauri, E.H., Nikogosian, I.K., Barszczus, H.G., 2002. Chlorine–potassium variations in melt inclusions from Raivavae and Rapa, Austral Islands: constraints on chlorine recycling in the mantle and evidence for brine-induced melting of oceanic crust. *Earth Planet. Sci. Lett.* 202, 525–540.
- Li, H., Hermann, J., 2015. Apatite as an indicator of fluid salinity: an experimental study of chlorine and fluorine partitioning in subducted sediments. *Geochim. Cosmochim. Acta* 166, 267–297.
- Li, H., Zhang, H., Ling, M.X., Wang, F.Y., Ding, X., Zhou, J.B., Yang, X.Y., Tu, X.L., Sun, W., 2011. Geochemical and zircon U–Pb study of the Huangmeijian A-type granite: implications for geological evolution of the Lower Yangtze River belt. *Int. Geol. Rev.* 53, 499–525.
- Li, C.Y., Zhang, H., Wang, F.Y., Liu, J.Q., Sun, Y.L., Hao, X.L., Li, Y.L., Sun, W.D., 2012a. The formation of the Dabaoshan porphyry molybdenum deposit induced by slab rollback. *Lithos* 150, 101–110.
- Li, H., Ling, M.X., Li, C.Y., Zhang, H., Ding, X., Yang, X.Y., Fan, W.M., Li, Y.L., Sun, W.D., 2012b. A-type granite belts of two chemical subgroups in central eastern China: indication of ridge subduction. *Lithos* 150, 26–36.
- Li, X.H., Li, Z.X., Li, W.X., Wang, X.C., Gao, Y., 2013. Revisiting the “C-type adakites” of the Lower Yangtze River Belt, central eastern China: in-situ zircon Hf–O isotope and

- geochemical constraints. *Chem. Geol.* 345, 1–15.
- Li, H., Ling, M.X., Ding, X., Zhang, H., Li, C.Y., Liu, D.Y., Sun, W.D., 2014. The geochemical characteristics of Haiyang A-type granite complex in Shandong, eastern China. *Lithos* 200–201, 142–156.
- Ling, M.X., Wang, F.Y., Ding, X., Hu, Y.H., Zhou, J.B., Zartman, R.E., Yang, X.Y., Sun, W., 2009. Cretaceous ridge subduction along the lower Yangtze River belt, eastern China. *Econ. Geol.* 104, 303–321.
- Lisowiec, K., Slaby, E., Götze, J., 2013. Cathodoluminescence (CL) of apatite as an insight into magma mixing in the granitoid pluton of karkonosze, Poland. July In: Proceedings of the Conference on Raman and Luminescence Spectroscopy in the Earth Sciences. Wien, Austria. pp. 3–6.
- Liu, Y., Hu, Z., Gao, S., Gunther, D., Xu, J., Gao, C., Chen, H., 2008. In situ analysis of major and trace elements of anhydrous minerals by LA-ICP-MS without applying an internal standard. *Chem. Geol.* 257, 34–43.
- Liu, C., Deng, J.F., Luo, Z.H., Tian, S.P., Zhang, Y., Zhong, C.T., Selby, D., Zhao, H.D., 2014. Post-batholith metallogenesis: evidence from Luming super large molybdenite deposit in Lesser Xing'an Range. *Acta Petrol. Sin.* 30, 3400–3418.
- Lou, Y.E., Du, Y.S., 2006. Characteristics and zircon SHRIMP U–Pb ages of the Mesozoic intrusive rocks in Fanchang, Anhui Province. *Geochimica* 35, 359–366.
- Macdonald, R., Bagiński, B., Dzierżanowski, P., Jokubauskas, P., 2013. Apatite-super-group minerals in UK Palaeogene granites: composition and relationship to host-rock composition. *Eur. J. Mineral.* 25, 461–471.
- Mao, J., Wang, Y., Lehmann, B., Yu, J., Du, A., Mei, Y., Li, Y., Zang, W., Stein, H.J., Zhou, T., 2006. Molybdenite Re–Os and albite <sup>40</sup>Ar/<sup>39</sup>Ar dating of Cu–Au–Mo and magnetite porphyry systems in the Yangtze River valley and metallogenic implications. *Ore Geol. Rev.* 29, 307–324.
- Mao, J., Xie, G., Duan, C., Pirajno, F., Ishiyama, D., Chen, Y., 2011. A tectono-genetic model for porphyry–skarn–stratabound Cu–Au–Mo–Fe and magnetite–apatite deposits along the Middle–Lower Yangtze River Valley, Eastern China. *Ore Geol. Rev.* 43, 294–314.
- Mao, M., Rukhlov, A.S., Rowins, S.M., Spence, J., Coogan, L.A., 2016. Apatite trace element compositions: a robust new tool for mineral exploration. *Econ. Geol.* 111, 1187–1222.
- Marks, M.A., Scharrer, M., Ladenburger, S., Markl, G., 2016. Comment on "Apatite: A new redox proxy for silicic magmas?". *Geochim. Cosmochim. Acta* 183, 267–270.
- Meinert, L.D., Dipple, G.M., Nicolescu, S., 2005. World skarn deposits. *Econ. Geol.* 299–336 100th Anniversary Volume.
- Meng, J.Y., 2014. The Porphyry Copper-polymetallic Deposit in Zhongdian, West Yunnan: Magmatism and Mineralization. PhD Thesis. China University of Geosciences, pp. 197 in Chinese with English abstract.
- Miles, A.J., Graham, C.M., Hawkesworth, C.J., Gillespie, M.R., Hinton, R.W., 2013. Evidence for distinct stages of magma history recorded by the compositions of accessory apatite and zircon. *Contrib. Mineral. Petrol.* 166, 1–19.
- Miles, A.J., Graham, C.M., Hawkesworth, C.J., Gillespie, M.R., Hinton, R.W., Bromiley, G.D., 2014. Apatite: a new redox proxy for silicic magmas? *Geochim. Cosmochim. Acta* 132, 101–119.
- Mitchell, R., Chudy, T., McFarlane, C.R., Wu, F.Y., 2017. Trace element and isotopic composition of apatite in carbonatites from the Blue River area (British Columbia, Canada) and mineralogy of associated silicate rocks. *Lithos* 286, 75–91.
- Nash, W.P., 1984. Phosphate Minerals in Terrestrial Igneous and Metamorphic Rocks. Phosphate minerals Springer, Berlin, Heidelberg, pp. 215–241.
- Pagé, L., Hattori, K., de Hoog, J.C., Okay, A.I., 2016. Halogen (F, Cl, Br, I) behaviour in subducting slabs: a study of lawsonite blueschists in western Turkey. *Earth Planet. Sci. Lett.* 442, 133–142.
- Pan, Y., Fleet, M.E., 2002. Compositions of the apatite-group minerals: substitution mechanisms and controlling factors. *Rev. Mineral. Geochem.* 48, 13–49.
- Pan, L.C., Hu, R.Z., Wang, X.S., Bi, X.W., Zhu, J.J., Li, C., 2016. Apatite trace element and halogen compositions as petrogenetic-metallogenic indicators: examples from four granite plutons in the Sanjiang region, SW China. *Lithos* 254, 118–130.
- Peacock, S.M., Rushmer, T., Thompson, A.B., 1994. Partial melting of subducting oceanic crust. *Earth Planet. Sci. Lett.* 121, 227–244.
- Prowatke, S., Klemme, S., 2006. Trace element partitioning between apatite and silicate melts. *Geochim. Cosmochim. Acta* 70, 4513–4527.
- Qin, K.Z., Zhai, M.G., Li, G.M., Zhao, J.X., Zeng, Q.D., Gao, J., Xiao, W.J., Li, J.L., Sun, S., 2017. Links of collage orogenesis of multiblocks and crust evolution to characteristic metallogenesis in China. *Acta Petrol. Sin.* 33, 305–325.
- Rapp, R.P., Xiao, L., Shimizu, N., 2002. Experimental constraints on the origin of potassium-rich adakites in eastern China. *Acta Petrol. Sin.* 18, 293–302.
- Reynard, B., 2013. Serpentine in active subduction zones. *Lithos* 178, 171–185.
- Schmidt, M.W., Poli, S., 2014. Devolatilization during subduction. In: Rudnick, R.L., Holland, H.D., Turekian, K.K. (Eds.), *The Crust, Treatise on Geochemistry*, second edition. Elsevier-Perigamon, Oxford, pp. 669–701.
- Sen, C., Dunn, T., 1995. Experimental modal metasomatism of a spinel lherzolite and the production of amphibole-bearing peridotite. *Contrib. Mineral. Petrol.* 119, 422–432.
- Sha, L.K., Chappell, B.W., 1999. Apatite chemical composition, determined by electron microprobe and laser-ablation inductively coupled plasma mass spectrometry, as a probe into granite petrogenesis. *Geochim. Cosmochim. Acta* 63, 3861–3881.
- Shannon, R.D., 1976. Revised effective ionic radii and systematic studies of interatomic distances in halides and chalcogenides. *Acta Crystallogr. A* 32, 751–767.
- Shao, J., Yang, H., Jia, B., Peng, M., 2012. Geological characteristics and ore-forming age of Luming Mo deposit in Heilongjiang Province. *Mineral Deposits* 31, 1301–1310.
- She, Y.W., Song, X.Y., Yu, S.Y., Chen, L.M., Zheng, W.Q., 2016. Apatite geochemistry of the Taihe layered intrusion, SW China: implications for the magmatic differentiation and the origin of apatite-rich Fe–Ti oxide ores. *Ore Geol. Rev.* 78, 151–165.
- Shi, P.H., Yang, Y.C., Ye, S.Q., Han, S.J., 2012. Geological and geochemical characteristics and genesis of ferromolybdenum deposit in Wudaoling, Heilongjiang Province. *Global Geology* 31, 262–270.
- Stronck, N.A., Haase, K.M., 2004. Chlorine in oceanic intraplate basalts: constraints on mantle sources and recycling processes. *Geology* 32, 945–948.
- Su, Y., Zheng, J., Griffin, W.L., Zhao, J., Suzanne, Y.O., Tang, H., Ping, X., Xiong, Q., 2013. Petrogenesis and geochronology of Cretaceous adakitic, I- and A-type granitoids in the NE Yangtze block: constraints on the eastern subsurface boundary between the North and South China blocks. *Lithos* 175, 333–350.
- Sun, W., Xie, Z., Chen, J., Zhang, X., Chai, Z., Du, A., Zhao, J., Zhang, C., Zhou, T., 2003. Os–Os dating of copper and molybdenum deposits along the middle and lower reaches of the Yangtze River. *China. Econ. Geol.* 98, 175–180.
- Sun, W.D., Binns, R.A., Fan, A.C., Kamenetsky, V.S., Wysoczanski, R., Wei, G.J., Hu, Y.H., Arculus, R.J., 2007. Chlorine in submarine volcanic glasses from the eastern Manus basin. *Geochim. Cosmochim. Acta* 71, 1542–1552.
- Sun, W.D., Ling, M.X., Chung, S.L., Ding, X., Yang, X.Y., Liang, H.Y., Fan, W.M., Goldfarb, R., Yin, Q.Z., 2012. Geochemical constraints on adakites of different origins and copper mineralization. *J. Geol.* 120, 105–120.
- Sun, W.D., Liang, H.Y., Ling, M.X., Zhan, M.Z., Ding, X., Zhang, H., Yang, X.Y., Li, Y.L., Ireland, T.R., Wei, Q.R., Fan, W.M., 2013. The link between reduced porphyry copper deposits and oxidized magmas. *Geochim. Cosmochim. Acta* 103, 263–275.
- Szopa, K., Gawęda, A., Müller, A., Sikorska, M., 2013. The petrogenesis of granitoid rocks unusually rich in apatite in the Western Tatra Mts. S-Poland, Western Carpathians). *Mineralogy and Petrology* 107, 609–627.
- Tollari, N., Barnes, S.J., Cox, R.A., Nabil, H., 2008. Trace element concentrations in apatites from the Sept-Îles Intrusive Suite, Canada—implications for the genesis of nelsonites. *Chem. Geol.* 252, 180–190.
- Turner, S., Foden, J., 2001. U, Th and Ra disequilibria, Sr, Nd and Pb isotope and trace element variations in Sunda arc lavas: predominance of a subducted sediment component. *Contrib. Mineral. Petrol.* 142, 43–57.
- Warner, S., Martin, R.F., Abdel-Rahman, A.F.M., Doig, R., 1998. Apatite as a monitor of fractionation, degassing, and metamorphism in the Sudbury igneous complex. *Ontario. Canad. Mineral.* 36, 981–999.
- Watson, E.B., 1980. Apatite and phosphorus in mantle source regions: an experimental study of apatite/melt equilibria at pressures to 25 kbar. *Earth Planet. Sci. Lett.* 51, 322–335.
- Watson, E.B., Green, T.H., 1981. Apatite/liquid partition coefficients for the rare earth elements and strontium. *Earth Planet. Sci. Lett.* 56, 405–421.
- Webster, J.D., 1990. Partitioning of F between H<sub>2</sub>O and CO<sub>2</sub> fluids and topaz rhyolite melt. *Contrib. Mineral. Petrol.* 104, 424–438.
- Webster, J.D., Piccoli, P.M., 2015. Magmatic apatite: a powerful, yet deceptive, mineral. *Elements* 11, 177–182.
- Webster, J.D., Tappen, C.M., Mandeville, C.W., 2009. Partitioning behavior of chlorine and fluorine in the system apatite–melt–fluid. II: Felsic silicate systems at 200 MPa. *Geochim. Cosmochim. Acta* 73, 559–581.
- Wu, F.Y., Sun, D.Y., Li, H.M., Wang, X.L., 2001. The nature of basement beneath the Songliao Basin in NE China: geochemical and isotopic constraints. *Phys. Chem. Earth Part A Solid Earth Geod.* 26, 793–803.
- Wu, F.Y., Lin, J.Q., Wilde, S.A., Zhang, X.O., Yang, J.H., 2005. Nature and significance of the Early Cretaceous giant igneous event in eastern China. *Earth Planet. Sci. Lett.* 233, 103–119.
- Wu, F.Y., Yang, J.H., Lo, C.H., Wilde, S.A., Sun, D.Y., Jahn, B.M., 2007a. The Heilongjiang Group: a Jurassic accretionary complex in the Jiamusi Massif at the western Pacific margin of northeastern China. *Isl. Arc* 16, 156–172.
- Wu, F.Y., Zhao, G.C., Sun, D.Y., Wilde, S.A., Yang, J.H., 2007b. The hulan group: its role in the evolution of the central asian orogenic belt of NE China. *J. Asian Earth Sci.* 30, 542–556.
- Wu, F.Y., Sun, D.Y., Ge, W.C., Zhang, Y.B., Grant, M.L., Wilde, S.A., Jahn, B.M., 2011. Geochronology of the Phanerozoic granitoids in northeastern China. *J. Asian Earth Sci.* 41, 1–30.
- Xie, F., Tang, J., Chen, Y., Lang, X., 2018. Apatite and zircon geochemistry of Jurassic porphyries in the Xionggun district, southern Gangdese porphyry copper belt: implications for petrogenesis and mineralization. *Ore Geol. Rev.* 96, 98–114.
- Xiong, X.L., Adam, J., Green, T.H., 2005. Rutile stability and rutile/melt HFSE partitioning during partial melting of hydrous basalt: implications for TTG genesis. *Chem. Geol.* 218, 339–359.
- Xiong, Q., Keppler, H., Audétat, A., Gudfinnsson, G., Sun, W., Song, M., Xiao, W., Yuan, L., 2009. Experimental constraints on rutile saturation during partial melting of metabasalt at the amphibolite to eclogite transition, with applications to TTG genesis. *Amer. Miner.* 94, 1175–1186.
- Yang, Y.C., Han, S.J., Sun, D.Y., Guo, J., Zhang, S.J., 2012. Geological and geochemical features and geochronology of porphyry molybdenum deposits in the Lesser Xing'an Range–Zhangguangcai Range metallogenic belt. *Acta Petrol. Sin.* 28, 379–390.
- Yang, Y.Z., Wang, Y., Ye, R.S., Li, S.Q., He, J.F., Siebel, W., Chen, F., 2017. Petrology and geochemistry of Early Cretaceous A-type granitoids and late Mesozoic mafic dikes and their relationship to adakitic intrusions in the lower Yangtze River belt, Southeast China. *Int. Geol. Rev.* 59, 62–79.
- Zafar, T., Leng, C.B., Zhang, X.C., Rehman, H.U., 2019. Geochemical attributes of magmatic apatite in the Kukaazi granite from western Kunlun orogenic belt, NW China: implications for granite petrogenesis and Pb–Zn (–Cu–W) mineralization. *J. Geochem. Explor.* 204, 256–269.
- Zeng, Q.D., Liu, J.M., Chu, S.X., Wang, Y.B., Sun, Y., Duan, X.X., Zhou, L.L., Qu, W.J., 2014. Re–Os and U–Pb geochronology of the Duobaoshan porphyry Cu–Mo–(Au) deposit, northeast China, and its geological significance. *J. Asian Earth Sci.* 79, 895–909.
- Zhang, C., Holtz, F., Ma, C., Wolff, P.E., Li, X., 2012. Tracing the evolution and distribution of F and Cl in plutonic systems from volatile-bearing minerals: a case study from the Liujiawa pluton (Dabie orogen, China). *Contrib. Mineral. Petrol.* 164,

- 859–879.
- Zhou, T.F., Wu, M., Fan, Y., Duan, C., Yuan, F., Zhang, L.J., Liu, J., Qian, B., Franco, P., David, R.C., 2011. Geological, geochemical characteristics and isotope systematics of the Longqiao iron deposit in the Lu-Zong volcano-sedimentary basin, Middle-Lower Yangtze (Changjiang) River Valley, Eastern China. *Ore Geol. Rev.* 43, 154–169.
- Zhu, C., Sverjensky, D.A., 1992. F-Cl-OH partitioning between biotite and apatite. *Geochim. Cosmochim. Acta* 56, 3435–3467.
- Zhu, J.C., Wang, R.C., Zhang, P.H., Xie, C.F., Zhang, W.L., Zhao, K.D., Xie, L., Yang, C., Che, X.D., Yu, A.P., Wang, L.B., 2009. Zircon U–Pb geochronological framework of qitianling granite batholith, middle part of Nanling Range, South China. *Science in China (Series D)* 52, 1279–1294.
- Zirner, A.L., Marks, M.A., Wenzel, T., Jacob, D.E., Markl, G., 2015. Rare earth elements in apatite as a monitor of magmatic and metasomatic processes: the Ilímaussaq complex, South Greenland. *Lithos* 228, 12–22.